NASA TN D-659

p 58

# TECHNICAL NOTE

D-659

## AN ANALYTICAL TREATMENT OF AIRCRAFT PROPELLER PRECESSION INSTABILITY

By Wilmer H. Reed III and Samuel R. Bland

Langley Research Center
Langley Field, Va.

NATIONAL AERONAUTICS AND SPACE ADMINISTRATION

WASHINGTON

January 1961

NATIONAL AERONAUTICS AND SPACE ADMINISTRATION

TECHNICAL NOTE D-659

# AN ANALYTICAL TREATMENT OF AIRCRAFT PROPELLER PRECESSION INSTABILITY

By Wilmer H. Reed III and Samuel R. Bland



## SUMMARY

An analytical investigation is made of a precession-type instability which can occur in a flexibly supported aircraft-engine—propeller combination. By means of an idealized mathematical model which is comprised of a rigid power-plant system flexibly mounted in pitch and yaw to a fixed backup structure, the conditions required for neutral stability are determined. The paper also examines the sensitivity of the stability boundaries to changes in such parameters as stiffness, damping, and asymmetries in the engine mount, propeller speed, airspeed, Mach number, propeller thrust, and location of pitch and yaw axes. Stability is found to depend strongly on the damping and stiffness in the system.

With the use of nondimensional charts theoretical stability boundaries are compared with experimental results obtained in wind-tunnel tests of an aeroelastic airplane model. In general, the theoretical results, which do not account for wing response, show the same trends as observed experimentally; however, for a given set of conditions calculated airspeeds for neutral stability are consistently lower than the measured values. Evidently, this result is due to the fact that wing response tends to add damping to the system.

## INTRODUCTION

A flexibly mounted aircraft-propeller—power-plant combination can, under certain conditions, develop a dynamic instability in which the propeller axis together with the power plant precesses in a diverging whirl-type motion. The existence of such a phenomenon was recognized and briefly investigated by Taylor and Browne as early as 1938 (ref. 1), but until recently has not been encountered in actual airplane configurations. An experimental investigation (unpublished) of this phenomenon was conducted on an aeroelastic model of an aircraft in the transonic dynamics tunnel at the Langley Research Center. These tests established the boundaries between stable and unstable operation of the system over a

range of such parameters as stiffness and damping of the engine mount, propeller speed, fuel loading, and so forth.

The aim of this paper is to present a parallel analytical investigation to shed further light on the basic mechanism of propeller whirl. The mathematical model treated represents a gross simplification of power-plant installations found in practice in that an isolated power-plant system is assumed to be flexibly mounted to a rigid backup structure and the only aerodynamic forces considered are those acting on the propeller. It is hoped that, by following a tractable solution of the propeller-precession problem, reduced to its most elementary form, important nondimensional parameters will be identified and suitable design criteria will evolve by which the stability characteristics of arbitrary propeller—power-plant configurations can be readily assessed.

## SYMBOLS

| | |
|---|---|
| $a_i, b_i$ | aerodynamic coefficients in equation (19) |
| $b$ | propeller blade section chord |
| $c_\theta$ | viscous damping coefficient |
| $c_{l_\alpha}$ | section lift-curve slope of propeller blade element |
| $C(k)$ | Theodorsen's oscillatory lift function |
| $C_m$ | pitching-moment coefficient, $\frac{M_Y}{\rho V^2 S' R}$ |
| $C_n$ | yawing-moment coefficient, $\frac{M_Z}{\rho V^2 S' R}$ |
| $C_T$ | thrust coefficient, $\frac{T}{4\rho V^2 R^2}$ |
| $C_Y$ | side-force coefficient, $\frac{F_Y}{\frac{1}{2}\rho V^2 S'}$ |
| $C_Z$ | vertical-force coefficient, $\frac{F_Z}{\frac{1}{2}\rho V^2 S'}$ |

| | |
|---|---|
| $D$ | dissipation function (see eq. (5)) |
| $E$ | angular momentum ratio, $\frac{I_X\Omega}{I_Y\omega_\theta}$ |
| $f_\theta, f_\psi$ | generalized aerodynamic force functions (see eq. (18)) |
| $F(k), G(k)$ | real and imaginary parts, respectively, of $C(k)$ |
| $F_Y, F_Z$ | aerodynamic forces along Y- and Z-axes, respectively |
| $g$ | structural damping coefficient |
| $\tilde{g}_\theta$ | structural damping in pitch required for neutral stability of system |
| $G$ | ratio of damping in yaw to damping in pitch, $\frac{g_\psi}{g_\theta}$ |
| $H$ | moment of inertia ratio, $\frac{\pi I_X}{I_Y}$ |
| $I_X$ | moment of inertia of propeller about axis of rotation |
| $I_Y, I_Z$ | moment of inertia of propeller—power-plant system about the pitch and yaw axes, respectively. |
| $J$ | propeller advance ratio, $\frac{V}{2nR}$ |
| $k$ | reduced frequency of propeller blade element, $\frac{\Omega b}{2U}$ |
| $k_\theta$ | reduced frequency of propeller—power-plant system, $\frac{\omega_\theta R}{V}$ |
| $l$ | distance from propeller plane of rotation to gimbal axes |
| $M$ | free-stream Mach number |
| $M_e$ | effective Mach number for propeller |

| | |
|---|---|
| $M_Y, M_Z$ | moments about Y- and Z-axes, respectively; positive sense is according to right-hand rule |
| n | propeller rotational speed, revolutions per second |
| $q_i$ | generalized coordinate in Lagrange's equation |
| $Q_{q_i}$ | generalized forces in Lagrange's equation where $q_i = \theta$ or $q_i = \psi$ |
| R | propeller radius |
| S' | propeller disk area |
| S | rotational stiffness of power-plant mount |
| t | time |
| T | kinetic energy of system or thrust |
| U | potential energy of system or helical velocity of propeller blade element |
| V | forward velocity |
| $V_e$ | equivalent air speed, $\sqrt{\frac{\rho}{\rho_{SL}}}\,V$ |
| $X_a$ | auxiliary coordinate in Euler axis transformation |
| $X_s, Y_s, Z_s$ | orthogonal space-fixed axis system (see fig. 2) |
| X,Y,Z | orthogonal body-fixed axis system (see fig. 2) |
| $\beta$ | geometric blade angle measured from plane of propeller rotation |
| $\beta_0$ | blade angle to zero lift measured from plane of propeller rotation |
| $\gamma$ | square root of ratio of yaw stiffness to pitch stiffness, $\sqrt{\frac{S_\psi}{S_\theta}}$ |

| | |
|---|---|
| $\delta$ | lag angle of oscillatory aerodynamic forces, $\tan^{-1}\left[\frac{-G(k)}{F(k)}\right]$ |
| $\delta W$ | virtual work |
| $\delta\theta, \delta\psi$ | virtual displacement in $\theta$ and $\psi$, respectively |
| $\zeta$ | ratio of viscous damping to critical damping |
| $\theta, \psi$ | pitch and yaw angles, respectively (see fig. 2) |
| $\overline{\theta}, \overline{\psi}$ | effective pitch and yaw angles, respectively (see eq. (11)) |
| $\kappa$ | ratio of air to structural moment of inertia, $\frac{\pi\rho R^5}{I_Y}$ |
| $\lambda$ | frequency ratio, $\frac{\omega}{\omega_\theta}$ |
| $\rho$ | air density |
| $\sigma$ | propeller solidity at 0.75R, $\frac{8b}{3\pi R}$ |
| $\tau$ | nondimensional distance traveled in propeller radii, $\frac{Vt}{R}$ |
| $\omega$ | frequency |
| $\omega_\theta$ | undamped natural frequency in pitch (at zero airspeed), $\sqrt{\frac{S_\theta}{I_Y}}$ |
| $\omega_\psi$ | undamped natural frequency in yaw (at zero airspeed), $\sqrt{\frac{S_\psi}{I_Y}}$ |
| $\omega_X, \omega_Y, \omega_Z$ | components of total angular velocity of system about the X-, Y-, and Z-axes, respectively |
| $\Omega$ | propeller rotational speed, radians/sec |

Subscripts:

| | |
|---|---|
| av | average value |
| 1,2 | forward and backward whirl modes, respectively |
| o | amplitude of oscillation (eq. (20)) |
| p | axes in plane of propeller rotation |
| q | differentiation with respect to $\frac{\dot{\theta}V}{R}$ |
| r | differentiation with respect to $\frac{\dot{\psi}V}{R}$ |
| rms | root mean square |
| SL | sea level |
| 0.75R | three-quarter propeller radius |
| $\theta,\psi$ | pitch and yaw directions, respectively |



Dots over symbols indicate differentiation with respect to $t$; primes denote differentiation with respect to $\tau$. Partial derivatives are denoted thusly: $C_{Y_\psi} = \frac{\partial C_Y}{\partial \psi}$, $C_{Y_\theta} = \frac{\partial C_Y}{\partial \theta}$, $C_{m_q} = \frac{\partial C_m}{\partial q}$, and so forth.

## DYNAMIC SYSTEM

### General Remarks

The problem to be considered in this paper is the dynamic aeroelastic stability of a rigid engine-propeller combination which is flexibly mounted so as to permit angular deflections of the propeller axis in a vertical (pitch) plane and a horizontal (yaw) plane. (See fig. 1.) The primary forces and moments to be considered are those associated with small amplitude pitching and yawing motions of the system. These forces and moments are functions of the inertia of the system, the elastic and damping properties of the mount, the gyroscopic moments due to propeller rotation, and the aerodynamic forces acting on the propeller. Thus, in contrast with actual airplane configurations, the wing structure on which the

power plant is mounted is assumed to be rigid and aerodynamic interference effects induced by the wing and adjacent propellers are ignored.

Consider first the free vibratory motions of the system when damping and aerodynamic forces are neglected. Assume that with a nonrotating propeller there is no coupling between the pitch and yaw degrees of freedom; that is, natural vibrations in pure pitch and pure yaw can occur independently. When the propeller is spinning, however, gyroscopic moments are produced wherein an angular pitching velocity causes a moment about the yaw axis and vice versa. Thus, the significant characteristic of this system is that the pitch and yaw modes are coupled by the action of gyroscopic moments. (The coupling of natural modes of aircraft structures due to propeller gyroscopic forces is investigated by Scanlan and Truman in ref. 2.) Gyroscopic coupling causes the natural frequency of the higher frequency uncoupled mode to increase and that of the lower frequency uncoupled mode to decrease. These modes are characterized by a precession-type motion. In the lower frequency mode the propeller axis precesses in a sense opposite to that of the propeller rotation and in the higher frequency mode the direction of precession and propeller rotation are the same. (See, for example, ref. 3.) In the present paper these modes will be referred to as the backward and forward whirl modes, respectively.

Although gyroscopic effects tend to couple the pitch and yaw degrees of freedom, gyroscopic action alone cannot lead to an oscillatory divergent-type instability because the mechanism for adding energy to the system is lacking. The mechanism for an energy transfer, either into or out of the system, can, however, be found in the aerodynamic forces acting on the propeller. When the propeller axis is deflected in pitch, an aerodynamic vertical force and a yawing moment about an axis in the plane of the propeller are developed which, for small deflections, are proportional to the pitch angle. In addition to these static forces, other aerodynamic forces and moments proportional to the rate of change of the angular deflection are also present. Some of these air forces drive and others resist motion of the previously discussed whirl modes. A condition of neutral stability, that is, a self-sustaining oscillation, is achieved when the energy input due to aerodynamic driving forces on the propeller is exactly balanced by the energy dissipated by internal damping in the system.

In the following analysis a modified Euler axis system together with Lagrange's formulation of the differential equations of motion are used. The equations of motion are cast in a nondimensional form from which approximate closed form expressions for conditions leading to neutral stability are derived and presented graphically.

## Equations of Motion

The coordinate system to be used in describing the motion of the propeller system is illustrated in figure 2. Two sets of orthogonal axes are considered. The $X_S$-, $Y_S$-, and $Z_S$-axes are fixed in space with the origin at the gimbal center and the X-, Y-, and Z-axes pitch and yaw with the power plant but do not rotate with the propeller. The Euler angles relating the body system to space-fixed coordinates are the pitch angle $\theta$ and the yaw angle $\psi$. The order of rotation in transforming from the space-fixed to the body-fixed coordinate system is as follows:

(a) Pitch through an angle $\theta$ about the space-fixed $Y_S$-axis to give $X_a$, $Y_S$, and Z coordinates.

(b) Yaw through an angle $\psi$ about the body-fixed Z-axis to give X, Y, and Z coordinates.



It can be seen that the Z-axis is constrained to lie in the $X_S$,$Z_S$ plane, that is, the vertical plane. Positive sense is in accordance with the right-hand rule and is indicated by the direction of arrows in the figure. The total angular velocity of the system is comprised of three vectors: a pitch rate $\dot{\theta}$, a yaw rate $\dot{\psi}$, and the propeller rotational speed $\Omega$ as indicated in figure 2. These vectors can be resolved into components $\omega_X$, $\omega_Y$, and $\omega_Z$ along the X-, Y-, and Z-axes, respectively.

The total kinetic of the system may be expressed

$$T = \frac{1}{2} I_X \omega_X^2 + \frac{1}{2} I_Y \omega_Y^2 + \frac{1}{2} I_Z \omega_Z^2 \tag{1}$$

where $I_X$ is the polar moment of inertia of the propeller, and $I_Y$ and $I_Z$ are moments of inertia of the complete system about the Y- and Z-axes, respectively. In the present analysis it is assumed that $I_Z = I_Y$. The kinetic energy of rotating engine parts could have also been included in equation (1); however, since this energy is generally small, it has been neglected in the present analysis. The relations between the angular velocities in the body-fixed coordinate system and those in the space-fixed coordinate system are for small pitch and yaw angles (see fig. 2)

$$\left.\begin{aligned} \omega_X &= \Omega + \dot{\theta} \sin \psi \approx \Omega + \dot{\theta}\psi \\ \omega_Y &= \dot{\theta} \cos \psi \approx \dot{\theta} \\ \omega_Z &= \dot{\psi} \end{aligned}\right\} \tag{2}$$

Thus, with equation (2), the expression for the total kinetic energy of the system for small pitch and yaw deflections about the gimbal axes becomes

$$T = \frac{1}{2} I_X\left(\Omega^2 + 2\Omega\dot{\theta}\psi\right) + \frac{1}{2} I_Y\left(\dot{\theta}^2 + \dot{\psi}^2\right) \tag{3}$$

The potential energy associated with pitching and yawing deflections is

$$U = \frac{1}{2} S_\theta \theta^2 + \frac{1}{2} S_\psi \psi^2 \tag{4}$$

where, as indicated in figure 1, $S_\theta$ and $S_\psi$ are the rotational spring constants for pitch and yaw, respectively.

Assume for the present that the damping in the engine mount system is defined by the structural damping concept commonly employed in flutter analysis. This type of damping produces a force in phase with the velocity of oscillation but proportional to the elastic restoring force. (See ref. 4.) A dissipation function applicable to structural damping with sinusoidal motion may be written

$$D = \frac{1}{2} \frac{S_\theta g_\theta}{\omega} \dot{\theta}^2 + \frac{1}{2} \frac{S_\psi g_\psi}{\omega} \dot{\psi}^2 \tag{5}$$

where $\omega$ is the frequency of oscillation, and $g_\theta$ and $g_\psi$ are the damping coefficients for the uncoupled pitch and yaw modes, respectively.

Although the choice of assuming a structural type of damping over, for example, viscous damping (force proportional to velocity), is at present arbitrary, since it is not known which is the better representation of the damping in the system, it will be shown later that the type of damping assumed does have a significant effect on the stability boundary.

The generalized forces are determined from the work done by the aerodynamic forces acting through a virtual displacement of each generalized coordinate. In terms of the aerodynamic moments about the gimbal axes the total work done is

$$\delta W = M_Y \delta\theta + M_Z \delta\psi \tag{6}$$

from which the generalized moments are determined to be

$$\left.\begin{aligned} Q_\theta &= \frac{\delta W}{\delta \theta} = M_Y \\ \text{and} \qquad Q_\psi &= \frac{\delta W}{\delta \psi} = M_Z \end{aligned}\right\} \tag{7}$$

where $M_Y$ and $M_Z$ are the propeller aerodynamic pitch and yaw moments about the gimbal axes.

Now, the Lagrange equation is

$$\frac{d}{dt}\left(\frac{\partial T}{\partial \dot{q}_i}\right) - \frac{\partial T}{\partial q_i} + \frac{\partial U}{\partial q_i} + \frac{\partial D}{\partial \dot{q}_i} = Q_{q_i} \tag{8}$$

where $q_i$ is the generalized coordinate $\theta$ or $\psi$. With the expressions for T, U, and D given by equations (3), (4), and (5), the differential equations of motion become

$$\left.\begin{aligned} I_Y\ddot{\theta} + I_X\Omega\dot{\psi} + S_\theta\theta + \frac{S_\theta g_\theta}{\omega}\dot{\theta} &= M_Y \\ I_Y\ddot{\psi} - I_X\Omega\dot{\theta} + S_\psi\psi + \frac{S_\psi g_\psi}{\omega}\dot{\psi} &= M_Z \end{aligned}\right\} \tag{9}$$

In order to determine $M_Y$ and $M_Z$ in equation (9), it is convenient to consider next the aerodynamic forces and moments that act on the propeller. As stated previously, when the axis of propeller rotation is inclined relative to the direction of the free stream, aerodynamic forces and moments are generated which, for small deflections, are proportional to the angle of inclination and rate of change of the inclination angle. It is convenient to express these aerodynamic forces and moments in terms of nondimensional propeller derivatives which can either be determined experimentally or calculated by methods such as that given by Ribner in reference 5. On the basis of Ribner's work the forces and the moments about axes in the propeller plane may be expressed as

$$\left.\begin{aligned} F_Z &= \tfrac{1}{2}\rho V^2 S' \left( C_{Z_\theta} \bar{\theta} + C_{Z_\psi} \bar{\psi} + C_{Z_r} \frac{\dot{\psi} R}{V} \right) \\ M_{Y,p} &= \rho V^2 S' R \left( C_{m_\psi} \bar{\psi} + C_{m_q} \frac{\dot{\theta} R}{V} \right) \\ F_Y &= \tfrac{1}{2}\rho V^2 S' \left( C_{Y_\psi} \bar{\psi} + C_{Y_\theta} \bar{\theta} + C_{Y_q} \frac{\dot{\theta} R}{V} \right) \\ M_{Z,p} &= \rho V^2 S' R \left( C_{n_\theta} \bar{\theta} + C_{n_r} \frac{\dot{\psi} R}{V} \right) \end{aligned}\right\} \tag{10}$$

The derivatives $C_{Z_\psi}$ and $C_{Y_\theta}$ are not considered in reference 5 but are included here because these derivatives have been observed experimentally and can be shown to have a significant stabilizing effect on propeller whirl. The angles $\bar{\theta}$ and $\bar{\psi}$ are the effective pitch and yaw angles between the propeller axis and the relative wind. They consist of two parts, a geometric angle and an angle due to translational velocity of the propeller hub. Thus,

$$\left.\begin{aligned} \bar{\theta} &= \theta - \frac{l\dot{\theta}}{V} \\ \bar{\psi} &= \psi - \frac{l\dot{\psi}}{V} \end{aligned}\right\} \tag{11}$$

where $l$ is the distance from the rotation axes (gimbal axes) to the plane of the propeller.

Because of symmetry the following reciprocal relations hold between the derivatives for pitching and yawing motions:

$$\left.\begin{aligned} C_{Z_\theta} &= -C_{Y_\psi} \\ C_{n_\theta} &= -C_{m_\psi} \\ C_{Y_\theta} &= C_{Z_\psi} \\ C_{m_q} &= C_{n_r} \\ C_{Y_q} &= C_{Z_r} \end{aligned}\right\} \tag{12}$$

With equation (10) the moments referred to the gimbal axes became

and

$$\left.\begin{aligned} M_Y &= M_{Y,p} - lF_Z \\ M_Z &= M_{Z,p} + lF_Y \end{aligned}\right\} \tag{13}$$

Before seeking solutions to these equations of motion it is advantageous to write equation (9) in terms of certain nondimensional parameters. For this purpose define a new independent variable $\tau$ as the distance traveled in propeller radii

$$\tau = \frac{Vt}{R} \tag{14}$$

Then, in terms of $\tau$, the derivatives in equation (9) become

$$(\dot{}) = \frac{V}{R}\frac{d(\ )}{d\tau} = \frac{V}{R}(\ )' \tag{15}$$

and

$$(\ddot{}) = \left(\frac{V}{R}\right)^2 \frac{d^2(\ )}{d\tau^2} = \left(\frac{V}{R}\right)^2 (\ )'' \tag{16}$$

With these substitutions and some algebraic manipulations the equations of motion may be written in the following nondimensional form:

$$\left.\begin{aligned} \theta'' + \frac{H}{J}\psi' + g_\theta \frac{k_\theta}{\lambda}\theta' + k_\theta{}^2\theta &= \kappa f_\theta \\ \psi'' - \frac{H}{J}\theta' + g_\theta \frac{Gk_\theta}{\lambda}\gamma^2\psi' + \gamma^2 k_\theta{}^2\psi &= \kappa f_\psi \end{aligned}\right\} \tag{17}$$

The nondimensional parameters in equation (17) are defined as follows:

$H$ ratio of polar moment of inertia of propeller to pitching moment of inertia of entire system, $I_X\pi/I_Y$

$J$ propeller advance ratio, $V/2nR$

$k_\theta$ reduced frequency, $\omega_\theta R/V$

$\gamma^2$ ratio of yaw stiffness to pitch stiffness, $\frac{S_\psi}{S_\theta} = \left(\frac{\omega_\psi}{\omega_\theta}\right)^2$

$G$ ratio of yaw damping to pitch damping, $g_\psi/g_\theta$

$\kappa$ ratio of mass moment of inertia of cylinder of air to pitching moment of inertia of the structure, $\pi\rho R^5/I_Y$

$\lambda$ frequency ratio, $\omega/\omega_\theta$

The generalized force functions are in the form

$$\left.\begin{aligned} f_\theta &= a_0\theta + a_1\theta' + a_2\theta'' + b_0\psi + b_1\psi' + b_2\psi'' \\ f_\psi &= -b_0\theta - b_1\theta' - b_2\theta'' + a_0\psi + a_1\psi' + a_2\psi'' \end{aligned}\right\} \tag{18}$$

where the a and b values in equation (18) are functions only of the propeller derivatives and the gimbal axis location. These coefficients are:

$$\left.\begin{aligned} a_0 &= -\frac{1}{2}\frac{l}{R} C_{Z_\theta} \\ a_1 &= C_{m_q} + \frac{1}{2}\left(\frac{l}{R}\right)^2 C_{Z_\theta} \\ a_2 &= -\frac{l}{R} C_{m_q} \\ b_0 &= C_{m_\psi} - \frac{1}{2}\frac{l}{R} C_{Z_\psi} \\ b_1 &= -\frac{l}{R}\left(\frac{1}{2} C_{Z_r} + b_0\right) \\ b_2 &= \frac{1}{2}\left(\frac{l}{R}\right)^2 C_{Z_r} \end{aligned}\right\} \tag{19}$$

It should be pointed out that the present analysis does not consider the apparent mass effects of air surrounding the propeller, which, if accounted for, would lead to additional terms in the $a_2$ and $b_2$ coefficients.

## Evaluation of Propeller Aerodynamic Derivatives

The aerodynamic derivatives used in this analysis were calculated for a propeller having the characteristics shown in figure 3. All derivatives were evaluated by Ribner's method (ref. 5) with the exception of $C_{Z_{\dot{\psi}}}$ which is not treated by Ribner. Such a derivative has, however, been observed experimentally and is believed, because of its stabilizing effect, to be of sufficient importance in the analysis of propeller whirl to merit some consideration. An approximate derivation of the derivative $C_{Z_{\dot{\psi}}}$ is presented in the appendix.



Because, as will be shown later, the thrust developed by a propeller has very minor effects on the aerodynamic derivatives of interest, wind-milling propellers were used here as they were in the experimental wind-tunnel tests (unpublished). From experimental data, the relation between the propeller advance ratio $J$ and the geometric blade angle $\beta_{0.75R}$ was determined and is plotted in figure 4. Figures 3 and 4 together with data in table I provide the information needed to calculate propeller derivatives for the windmilling case.

The calculated propeller derivatives plotted against $\beta_{0.75R}$ are presented in figure 5. Also shown for comparison are the derivatives calculated for a thrusting propeller for $\beta_{0.75R} = 46^{\circ}$.

In order to account for the effect of Mach number on the coefficients in figure 5, an approximate Mach number correction factor $\frac{1}{\sqrt{1 - M_e^2}}$, calculated by the method of reference 5, is shown plotted in figure 6 against $\beta_{0.75R}$ for various free-stream Mach numbers. (The symbol $M_e$ represents an effective Mach number on the propeller.) This correction is to be applied as a multiplying factor to the derivatives determined for the incompressible case.

## DYNAMIC STABILITY CONSIDERATIONS

### Conditions for Neutral Stability

In order to find the conditions for which the system becomes neutrally stable, sinusoidal motion is specified for $\theta$ and $\psi$ in the equations of motion. Thus, when

$$\theta(t) = \theta_o e^{i\omega t}$$

or in nondimensional form

$$\left.\begin{aligned} \theta(\tau) &= \theta_o e^{i\lambda k_\theta \tau} \\ \psi(\tau) &= \psi_o e^{i\lambda k_\theta \tau} \end{aligned}\right\} \qquad (20)$$

and

are substituted into equation (17), a nontrivial solution is obtained when the determinant of the coefficients

$$\begin{vmatrix} \left[k_\theta^2(1-\lambda^2) + \kappa\left(\lambda^2 k_\theta^2 a_2 - a_0\right)\right] + i\left[g_\theta k_\theta^2 - \kappa\lambda k_\theta a_1\right] & \left[\kappa\left(\lambda^2 k_\theta^2 b_2 - b_0\right)\right] + i\left[\lambda k_\theta\left(\frac{H}{J} - \kappa b_1\right)\right] \\ \left[\kappa\left(b_0 - \lambda^2 k_\theta^2 b_2\right)\right] + i\left[\lambda k_\theta\left(\kappa b_1 - \frac{H}{J}\right)\right] & \left[k_\theta^2(\gamma^2 - \lambda^2) + \kappa\left(\lambda^2 k_\theta^2 a_2 - a_0\right)\right] + i\left[g_\theta G k_\theta^2 \gamma^2 - \kappa\lambda k_\theta a_1\right] \end{vmatrix} \qquad (21)$$

is set equal to zero.

When equation (21) is expanded and the resulting real and imaginary parts equated to zero, it is found that in the real equation $g_\theta$ always appears either multiplied by itself or by one of the aerodynamic terms. By neglecting these second-order terms, which appears to be a valid assumption for the range of $\kappa$- and g-values of interest, the real part of the expanded determinant becomes a quadratic in $\lambda^2$. The two roots of $\lambda^2$, corresponding to the forward and backward whirl modes, are, respectively,

$$\left.\begin{aligned} \lambda_1^2 &= \frac{-B + \sqrt{B^2 - 4AC}}{2A} \\ \lambda_2^2 &= \frac{-B - \sqrt{B^2 - 4AC}}{2A} \end{aligned}\right\} \qquad (22)$$

where

$$A = k_\theta^4\left[1 - 2\kappa a_2 + \overline{\kappa^2\left(a_2^2 + b_2^2\right)}\right]$$

$$B = k_\theta^2\left[-\left(1 + \gamma^2\right)k_\theta^2 - \left(\frac{H}{J}\right)^2 + 2\kappa a_0\right] + k_\theta^2\kappa\left[\overline{2b_1\frac{H}{J}} + \overline{a_2\left(1 + \gamma^2\right)k_\theta^2}\right.$$

$$\left. - \overline{2\kappa\left(a_0a_2 + b_0b_2\right)} - \overline{\kappa\left(a_1^2 + b_1^2\right)}\right]$$

$$C = \gamma^2k_\theta^4 - \kappa a_0\left(1 + \gamma^2\right)k_\theta^2 + \kappa\left(a_0^2 + b_0^2\right)$$

The terms beneath the bars are, for conditions of the present analysis, considered to be negligible and have been ignored.

The amount of damping required for neutral stability, is found by equating the imaginary part of the expanded determinant to zero and solving for $g_\theta$

$$\tilde{g}_\theta = \frac{\lambda\kappa}{k_\theta}\left[\frac{a_1\left(k_\theta^2 - 2\lambda^2k_\theta^2 + \gamma^2k_\theta^2\right) + 2\frac{H}{J}\left(b_0 - b_2\lambda^2k_\theta^2\right) - 2\kappa\left(a_0a_1 + b_0b_1\right) + 2\kappa\left(a_1a_2 + b_1b_2\right)\lambda^2k_\theta^2}{k_\theta^2\left(\gamma^2 - \lambda^2\right) + k_\theta^2\left(1 - \lambda^2\right)\gamma^2G + \kappa\left(a_2\lambda^2k_\theta^2 - a_0\right)\left(1 + \gamma^2G\right)}\right] \qquad (23)$$

The $\sim$ superscript is used to denote a neutral stability condition.

The procedure for determining stability boundaries from equations (22) and (23) is as follows: For a given set of parameters equation (22) is first evaluated to give the forward and backward whirl frequencies $\lambda_1$ and $\lambda_2$. Only positive roots are used in order to be

consistent with the motion assumed in equation (20). With these frequencies substituted separately into equation (23) the damping required for neutral stability is determined for each whirl mode.

Figure 7 shows typical plots of $\lambda_{1,2}$ and $\tilde{g}_{\theta_{1,2}}$ against the parameter $V/R\omega_\theta$ for a system having symmetrical damping ($G = 1.0$) and asymmetrical stiffness ($\gamma = 1.4$). Other parameters used are presented in figure 5 and table I. If for a given set of conditions the system damping is less than that indicated by the appropriate $\tilde{g}_\theta$ stability boundary in figure 7, the system will be unstable. Since the damping in an actual physical system is always positive, the figure shows that propeller whirl, if encountered, will stem from the backward whirl mode.

In order to gain a better understanding of the significance of various terms in the stability boundary equation, it is instructive to make further approximations to arrive at a considerably simpler expression for $\tilde{g}_\theta$. For this purpose consider the special case of equal stiffness and damping in the pitch and yaw directions, that is, $\gamma = 1.0$ and $G = 1.0$. If in the frequency equation (eq. (22)) all aerodynamic terms are neglected and an angular momentum ratio, defined as $E = \dfrac{I_X\Omega}{I_Y\omega_\theta}$ is assumed to be less than unity, the frequency relation reduces to

$$\left.\begin{aligned} \lambda_1 &\approx 1 + \frac{E}{2} \\ \lambda_2 &\approx 1 - \frac{E}{2} \end{aligned}\right\} \tag{24}$$

When these relations for $\lambda$ are substituted into equation (23) and the aerodynamic terms of lesser importance dropped, the following approximate expressions for $\tilde{g}_\theta$ are obtained

Forward whirl:

$$\tilde{g}_{\theta_1} = \frac{\kappa}{k_\theta}\left[\left(1 + \frac{E}{2}\right)a_1 - \frac{b_0}{k_\theta}\right] \tag{25}$$

Backward whirl:

$$\tilde{g}_{\theta_2} = \frac{\kappa}{k_\theta}\left[\left(1 - \frac{E}{2}\right)a_1 + \frac{b_0}{k_\theta}\right] \tag{26}$$

Where, as in equation (19),

$$a_1 = C_{m_q} + \frac{1}{2}\left(\frac{l}{R}\right)^2 C_{Z_\theta}$$

$$b_0 = C_{m_\psi} - \frac{1}{2}\frac{l}{R} C_{Z_\psi}$$



Figure 8 indicates that these approximate expressions for $\lambda_{1,2}$ and $\tilde{g}_{\theta_{1,2}}$ agree very closely with the more exact equations (eqs. (22) and (23)) for the case under consideration, that is, a symmetrical distribution of stiffness and damping in the system.

Note that for the aerodynamic coefficients and gimbal axes location used (see fig. 5 and table I) the term $a_1$ is always negative and the term $b_0$ is always positive. Therefore, equations (25) and (26) show that for these conditions the damping required for neutral stability can become positive only for the backward mode. This result indicates that, if an instability occurs, it must develop in the backward whirl mode, a conclusion consistent with wind-tunnel results and the theory in reference 1.

## Subcritical and Supercritical Response

The equation for $\tilde{g}_\theta$ defines only the boundary between stable and unstable operation of the system and does not necessarily indicate the degree of stability or the severity of an instability when the actual damping is other than $\tilde{g}_\theta$.

As a qualitative indication of the behavior of the system for conditions on either side of the boundary, figure 9 illustrates some typical transient motions of the system for three values of damping. These curves, obtained on an analog computer, represent the paths traced by the propeller hub after being released from an initial lateral displacement. The cases shown are for equal stiffness and damping in the pitch and yaw directions. Note that the oscillatory motion is damped when $g_\theta = 0.08$, neutrally stable when $g_\theta = \tilde{g}_{\theta_2} = 0.06$, and divergent when $g_\theta = 0.04$.

The path described by the propeller hub may be considered as the superposition of two rotating vectors. One vector rotates about the

origin of the $Y_s, Z_s$ coordinates in a clockwise direction at the frequency of the forward whirl mode and the other vector rotates in a counterclockwise direction at a lower frequency corresponding to the backward whirl mode. For the particular initial condition used in figure 9 a corner occurs in the path each time the two rotating vectors point in the same direction. Note that in each case the backward whirl (counterclockwise) is the predominant mode and that the forward mode is heavily damped.

## Generalized Stability Boundary Plots

Description.- Figure 10 gives the effects of varying some of the nondimensional parameters considered in this analysis. These charts show $\tilde{g}_{\theta_2}$ plotted against the parameter $V/R\omega_\theta$ for a range of values of J, $\gamma$, and G. Only $\tilde{g}_\theta$ values for the backward whirl mode are presented because in all cases considered this was the mode in which the instability occurred. In these calculations the following conditions were assumed: windmilling propeller, incompressible flow, fixed pitch, and yaw rotation axes at the position of the model gimbal axes ($l/R = 0.3778$), and inertia parameters corresponding to the system at a flight altitude of 15,000 feet standard atmosphere. (See fig. 5 and table I for numerical values.)

Before utilizing these nondimensional plots it is of interest to consider trends that might be expected when conditions are different from those assumed in figure 10. Specifically, the effects of varying the air density, Mach number, propeller thrust, gimbal axes location, and the assumed nature of the damping in the engine mounts are discussed.

Air density.- First consider the effect of air density on the stability boundary. For the case of symmetrical stiffness and damping it is seen from the approximate relation given by equation (26) that $\tilde{g}_\theta$ is simply proportional to the nondimensional moment of inertia parameter $\kappa = \frac{\pi\rho R^5}{I_Y}$. Thus, in order to determine approximately the stability boundary for altitudes other than that assumed in the figure, the value of $\tilde{g}_{\theta_2}$ read from figure 10 can be multiplied by the ratio of the air density at the desired altitude to the density used in this analysis (15,000 feet).

Mach number.- The effect of Mach number on the stability boundary is indicated in figure 11 for $J = 2.6$, $G = 1.0$, and $\gamma = 1.0$. These results were obtained by applying the Mach number correction shown in figure 6 to the propeller aerodynamic derivatives. Note that for a

given mount damping and stiffness (stiffness is proportional to $\omega_\theta^2$) the effect of increasing Mach number is to reduce the velocity for which the system becomes unstable. The higher the Mach number the more sensitive the system becomes to this unfavorable effect.

Propeller thrust.- Shown in figure 12 is a comparison of the calculated stability boundary for a thrusting and a windmilling propeller. The propeller coefficients used for the thrusting case are those plotted in figure 5 and correspond to cruising thrust at 15,000 feet altitude with an advance ratio $J = 2.22$. Note that the differences between these two stability boundaries are hardly discernible in the figure. Consequently, there appears to be good justification for using windmilling in place of thrusting propellers in the wind-tunnel tests (unpublished).

Gimbal axes location.- The stability boundaries shown in figure 10 are for gimbal axes located 0.3778 propeller radius behind the propeller plane of rotation. In order to examine the sensitivity of these boundaries to gimbal axes location, the parameter $l/R$ was varied in figure 13 over a range from 0 to 0.80. In these calculations it was assumed that only the aerodynamics were affected by changes in $l/R$, the moments of inertia remaining fixed. These results indicate that increasing the distance between the propeller plane and the gimbal axes has a stabilizing effect. Note also from equations (25) and (26) that as this distance is increased beyond about 2 propeller radii the sign of $b_0$ changes from positive to negative. In this case, whirl instability would be expected to develop in the forward whirl mode; however, limited calculations indicate that before reaching this condition, which occurs at very large values of $V/R\omega_\theta$, the system would probably suffer a static aeroelastic divergence.

Damping concept.- As pointed out earlier, the type of damping considered for the system produces a force proportional to the amplitude of displacement but independent of the velocity of motion. This concept of damping has been found to give a better description of damping measured on aircraft structures than does viscous damping which produces a damping force proportional to velocity. It is of interest, however, to compare the stability boundaries determined for these two familiar types of damping. For a sinusoidal pitching motion of frequency $\omega$, it can be shown that, for a given amplitude of oscillation, structural damping and viscous damping dissipate the same energy when

$$g_\theta = 2\zeta_\theta \frac{\omega}{\omega_\theta} \tag{27}$$

where

$$\zeta_\theta = \frac{c_\theta}{2I_Y\omega_\theta}$$

is the viscous damping coefficient relative to critical damping. In this equation $\omega_\theta$ is the undamped natural pitching frequency of the system with a nonrotating propeller and $\omega$ represents the damped natural frequency. If the propeller is not rotating and the system is lightly damped, $\omega \approx \omega_\theta$ and therefore from equation (27) structural and viscous damping are simply related as $g_\theta \approx 2\zeta_\theta$. When the propeller is spinning, however, because of gyroscopic coupling, $\omega$ may be considerably different from $\omega_\theta$, in which case the damping forces will depend on whether the damping is of a viscous or of a structural nature.

An indication is given in figure 14 of the shift in the stability boundary due to using a viscous rather than a structural description of the damping in the engine mount. The viscous damping curve was computed by replacing $g_\theta$ in equation (9) by the equivalent expression given in equation (27) (similarly for $g_\psi$). As is evident in the figure, viscous damping is not as effective as structural damping in the prevention of instability since the unstable mode, being the backward whirl mode, has a frequency less than that for the case of a nonrotating propeller. Therefore, to absorb a given amount of energy, the viscous damping coefficient $2\zeta_\theta$ must be greater than the structural damping coefficient $g_\theta$.

## Effects of Unsymmetrical Stiffness and Damping

Experimental results for the stability boundaries of systems having different relative lateral and vertical stiffnesses are sometimes correlated by an effective stiffness defined as the root mean square of the two stiffnesses

$$S_{rms} = \sqrt{\frac{S_\theta^2 + S_\psi^2}{2}} \tag{28}$$

Thus, within the accuracy of this criterion, the stability characteristics of systems having arbitrary relative stiffness in pitch and yaw can be inferred from the behavior of a symmetrical system having the same root-mean-square stiffness. It is of interest to determine the scatter that might be expected when using this method of correlation.

These results would provide an indication of the range of stiffness ratios over which the previously developed simplified stability boundary equation for a symmetrical system (eq. (26)) would be applicable.

Figure 15(a) presents a family of stability boundaries showing the variation of root-mean-square stiffness with equivalent airspeed for various ratios of yawing stiffness to pitching stiffness. A structural damping of 0.03 was assumed in both pitch and yaw and a propeller speed of 1,020 revolutions per minute was used. These plots were determined graphically from the nondimensional working charts in figure 10. Figure 15(a) indicates that at the lower root-mean-square stiffness values, the root-mean-square stiffness criterion is a reasonable criterion to use in defining the stability boundary over the range of stiffness ratios shown. Also, the figure points up the interesting fact that, for a given root-mean-square stiffness, it is the symmetrical system $\left(\frac{S_\psi}{S_\theta} = 1.0\right)$ that has the lowest critical airspeed. Thus, for a given root-mean-square stiffness, engine-mount stiffness asymmetries appear to produce a beneficial effect; however, the range of parameters for which this conclusion applies has not been established.

The structural damping in figure 15(a) was assumed to be equal for both modes. In order to illustrate the effect of unsymmetrical damping on the stability boundary, the average damping

$$g_{av} = \frac{g_\theta + g_\psi}{2} \tag{29}$$

was held constant at 0.03 and the damping ratio G was varied from 0.5 to 2.0. The results are presented in figure 15(b) which shows stability boundary plots of stiffness ratio against equivalent airspeed for a root-mean-square stiffness of $7.36 \times 10^6$ and $12.3 \times 10^6$ in-lb/radian. The G = 1.0 curve represents a cross plot of figure 15(a). If the stiffness is symmetrical, the average damping is a good measure of the effective damping of the system since the stability boundary for each damping ratio shown intersects at $\frac{S_\psi}{S_\theta} = 1.0$. However, when the stiffness ratio is different from unity and the average damping held constant, it is seen that the critical speed is increased when the damping in the less stiff direction exceeds that in the more stiff direction.

## COMPARISON OF THEORY WITH EXPERIMENT

### General Trends

In the present sections, a comparison is made between the results of this analysis and experimentally determined propeller whirl characteristics. Although the analysis shows the same trends as the experimental data, close agreement is not to be expected since the theory considers only an isolated nacelle, and thus neglects wing motion and aerodynamic effects of the wing and adjacent propellers. It should also be noted that the actual structural damping present during the experimental tests could not be precisely determined because, in order to obtain consistent results, it was necessary to measure damping with the nacelle system mounted to a rigid backstop rather than to the flexible wing structure. Also aerodynamic drag loads on the gimbal bearing may tend to increase the damping above that measured in still air.

### Whirl Frequency

A comparison of calculated and measured whirl frequencies against propeller speed is shown in figure 16 for two stiffness ratios. Aerodynamic forces have a small effect on the frequency of whirl and were neglected in determining the theoretical curves shown. The figure clearly indicates that the measured whirl frequencies stem from the backward whirl mode.

### Propeller-Speed—Airspeed Stability Boundary

Figure 17 shows the measured and calculated effects of propeller speed on the stability boundary. The stiffness is $8.09 \times 10^6$ inch-pounds per radian and the structural damping is approximately $g_\theta \approx 0.014$. The two experimental stability boundaries are for the number 4 (outboard) nacelle and the number 3 (inboard) nacelle. Thus, the three curves in the figure represent three different levels of flexibility in the nacelle mount backup structure. Nacelle 4, being located outboard on the wing, has a less rigid backup structure than nacelle 3. The theoretical curve is, of course, a limiting case wherein the backup structure is completely rigid. From these curves, it may be concluded that the effect of increasing wing flexibility in this case is to increase the airspeed for which the system becomes neutrally stable. Also, both theory and experiment show that an increase in propeller speed is accompanied by a reduction in critical airspeed.

### Damping-Airspeed Stability Boundary

The variation of structural damping required for neutral stability with airspeed is shown in figure 18 for conditions of a propeller speed of 1,020 revolutions per minute and a stiffness of $8.09 \times 10^6$ inch-pounds per radian. If, for a given airspeed, the structural damping is greater than that indicated by the stability boundary, disturbed motions of this system will dampen out. If, on the other hand, the damping of the mount falls below the stability boundary curve, disturbed motions will develop into an oscillatory divergence in the backward whirl mode. Here, as in figure 17, the same indications regarding the effects of wing flexibility are evident. Note that, for low values of structural damping, the slope of the stability boundary curve is small (see fig. 10) and therefore, in this region, the critical airspeed is very sensitive to changes in damping.



### Stiffness-Damping Stability Boundary

As a final comparison of theory (rigid backup) and experiment (unpublished), figure 19 shows the variation of root-mean-square stiffness with damping required for neutral stability at $V_e = 304$ knots. The theoretical curve is for a propeller speed of 1,020 revolutions per minute and symmetrical stiffness and damping. The experimental results, are for the number 4 nacelle and fall within the band indicated by the crosshatched area. The apparent scatter in the experimental results is to be expected since the data shown represent a composite of all data points irrespective of propeller speed or relative stiffness and damping in the pitch and yaw directions. The theoretical results are again conservative in that for a given damping a higher stiffness is required for stability by the theory than was determined experimentally.

## CONCLUDING REMARKS

An analytical investigation has been made of the dynamic stability of an aircraft engine-propeller combination flexibly mounted to a rigid backup structure. The conditions for which the system undergoes self-excited precession (propeller whirl) are examined. Results are presented in the form of nondimensional plots from which stability boundaries for various combinations of stiffness of the power-plant mount, structural damping, and propeller speed can be readily determined. Stability is found to depend strongly on the damping and stiffness in the system. It is found that the theoretical results, which do not account

for the effects of wing response, show the same trends as observed in wind-tunnel tests of an aeroelastic model but indicate instability for lower velocities than do the model tests. Thus, wing flexibility appears to increase the damping of the system.

Langley Research Center,
National Aeronautics and Space Administration,
Langley Field, Va., November 14, 1960.

# APPENDIX

## PROPELLER VERTICAL FORCE DUE TO YAW DERIVATIVE $C_{Z_\psi}$

The existence of the derivative $C_{Z_\psi}$ can be attributed to phase lags of aerodynamic forces acting on the propeller. When the propeller axis is deflected relative to the free-stream direction, as in yaw, the angle of attack of a blade element varies harmonically at a fundamental frequency corresponding to that of the propeller rotational speed. Because of an aerodynamic phase lag associated with these angle-of-attack oscillations, the total force vector in the plane of rotation due to a yaw angle has a small vertical component as well as the usual horizontal component. Thus, if the side force due to yaw undergoes a lag $\delta$, the vertical force due to yaw may be expressed as

$$C_{Z_\psi} = C_{Y_\psi} \tan \delta \tag{A1}$$

A rough estimate of the magnitude of $\delta$ can be obtained by simply modifying the slope of the section lift curve of the propeller blade element by Theodorsen's $C(\kappa)$ function (ref. 4) for oscillatory flow

$$C(k) = F(k) + iG(k) \tag{A2}$$

The lag angle $\delta$ is given by the expression

$$\delta = \tan^{-1}\left[\frac{-G(k)}{F(k)}\right] \tag{A3}$$

This expression for $\delta$ must, at best, be viewed as a very approximate one since $C(k)$ is derived on the assumption that the shed vortices be in a plane whereas in the case of a propeller the wake is shed in a helical pattern.

The real and imaginary parts of $C(k)$ are functions of a reduced frequency $k = \frac{\Omega b}{2U}$ which, of course, varies along the propeller radius. For the present purpose assume an effective reduced frequency for the propeller to be that of the blade element at 0.75R. It can be shown that the velocity of this blade element along a helical path expressed in terms of the rotational speed and the advance ratio is

$$U_{0.75R} = \Omega R\sqrt{\left(\frac{3}{4}\right)^2 + \left(\frac{J}{\pi}\right)^2} \tag{A4}$$

Hence, the effective reduced frequency becomes

$$k = \frac{b_{0.75R}}{2R\sqrt{\left(\frac{3}{4}\right)^2 + \left(\frac{J}{\pi}\right)^2}} \tag{A5}$$

From tabulated values of $C(k)$ the phase lag and thus $C_{Z_\psi}$ (eq. (A1)) can be determined for specified values of $J$. It is found that the phase lag varies from $11.9^\circ$ to $9.4^\circ$ over a $J$ range of from 1.8 to 4.2.

## REFERENCES

1. Taylor, E. S., and Browne, K. A.: Vibration Isolation of Aircraft Power Plants. Jour. Aero. Sci., vol. 6, no. 2, Dec. 1938, pp. 43-49.

2. Scanlan, R. H., and Truman, John C.: The Gyroscopic Effect of a Rigid Rotating Propeller on Engine and Wing Vibration Modes. Jour. Aero. Sci., vol. 17, no. 10, Oct. 1950, pp. 653-659, 666.

3. Den Hartog, J. P.: Mechanical Vibrations. Third Ed., McGraw-Hill Book Co., Inc., 1947.

4. Scanlan, Robert H., and Rosenbaum, Robert: Introduction to the Study of Aircraft Vibration and Flutter. The Macmillan Co., 1951.

5. Ribner, Herbert S.: Propellers in Yaw. NACA Rep. 820, 1945. (Supersedes NACA ARR 3L09.)

TABLE I

SUMMARY OF NACELLE-PROPELLER CHARACTERISTICS USED IN ANALYSIS

| | |
|---|---|
| $I_X$, slug-ft$^2$ | 175 |
| $I_Y$, slug-ft$^2$ | 1,375 |
| R, ft | 6.75 |
| $b_{0.75R}$, ft | 1.458 |
| $\rho$, slug/ft$^3$ | 0.001496 |
| $l/R$ | 0.3778* |
| $\sigma$ | 0.1834 |
| $c_{l_\alpha}$ | $2\pi$ |
| Spinner-nacelle fineness ratio | 6.0** |
| Spinner radius/Propeller radius | 0.181** |

*In figure 13 $l/R$ is varied.
**Values assumed for use in reference 5.

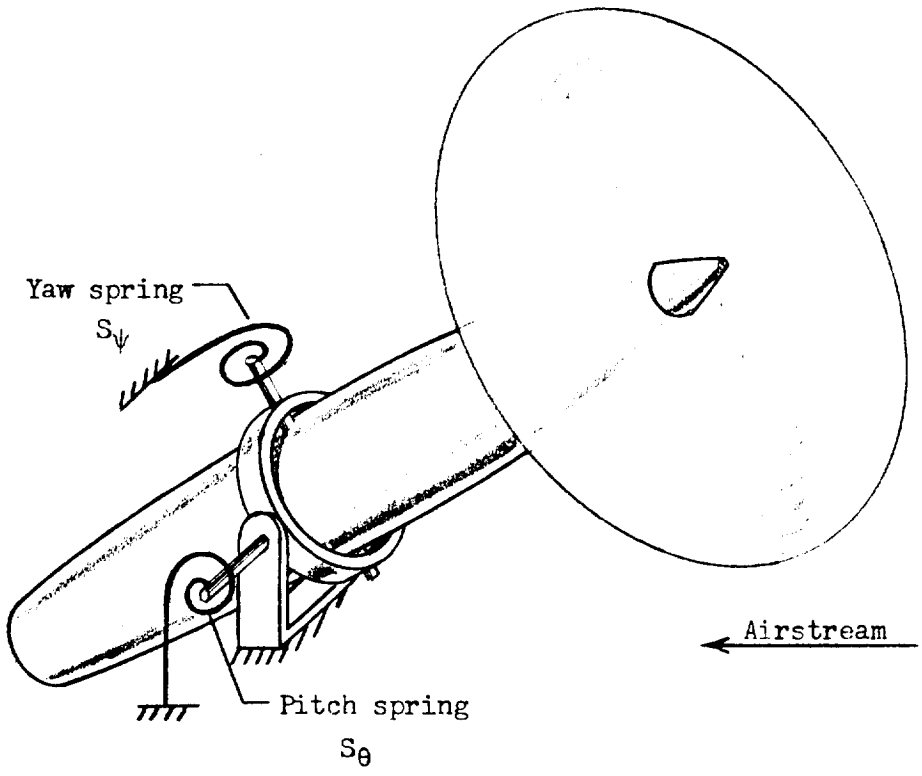


Figure 1.- Schematic representation of the idealized dynamic system considered in the analysis.

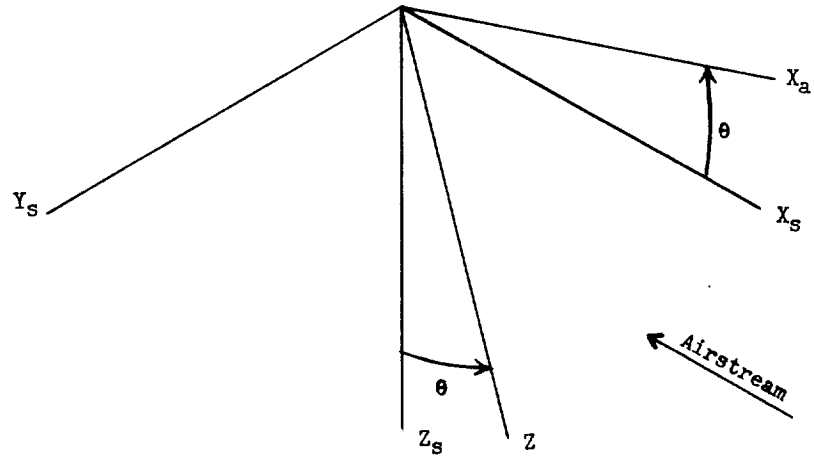


(a) $\theta$ rotation.

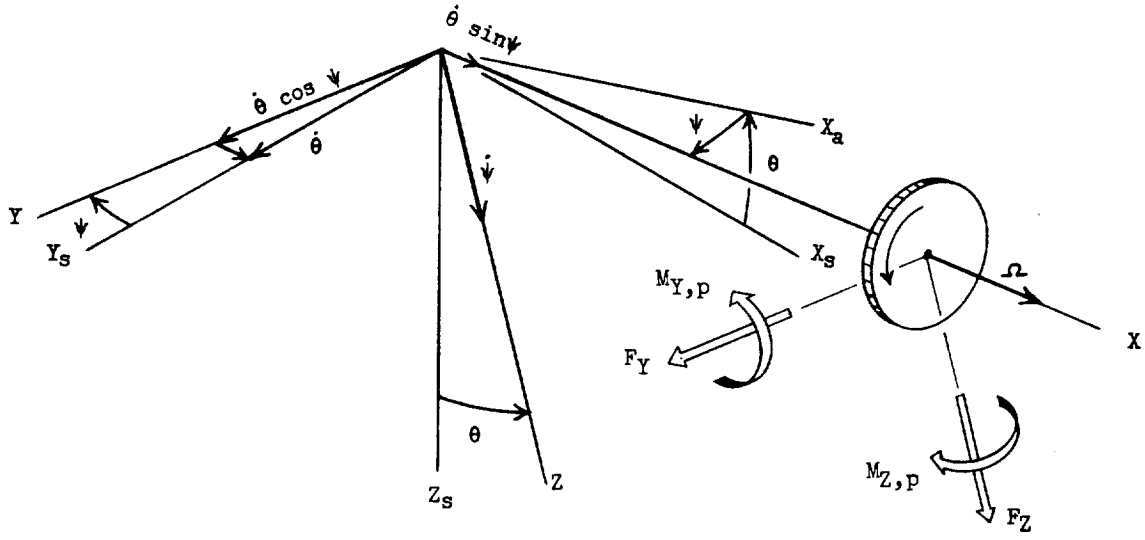


(b) $\psi$ rotation.

Figure 2.- Coordinate system showing Euler axis transformation.

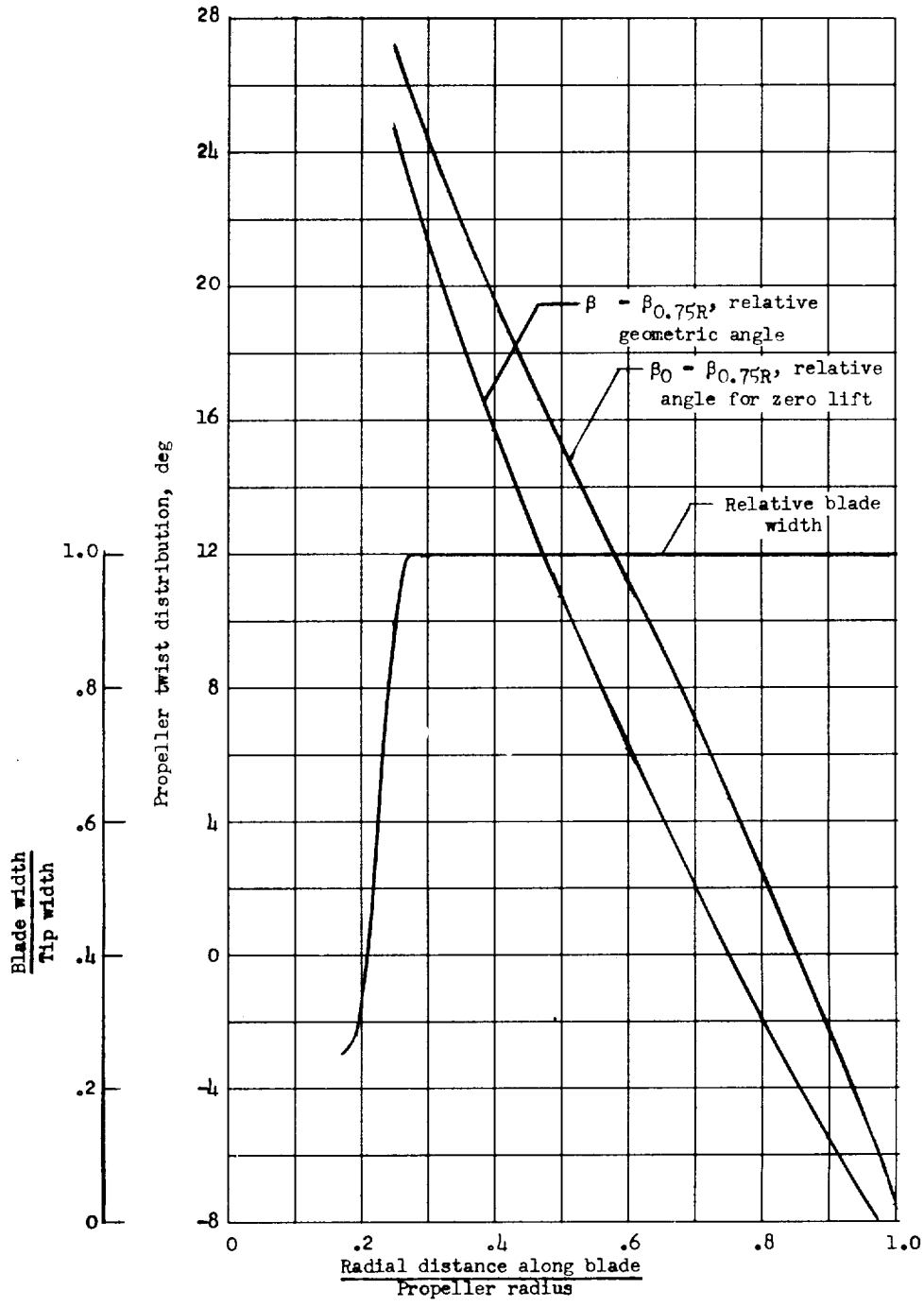


Figure 3.- Distribution of propeller twist angle and blade width for the airplane propeller of this analysis. Propeller dimensions: blade tip width, 1.458 ft; propeller radius, 6.75 ft; number of blades, 4.

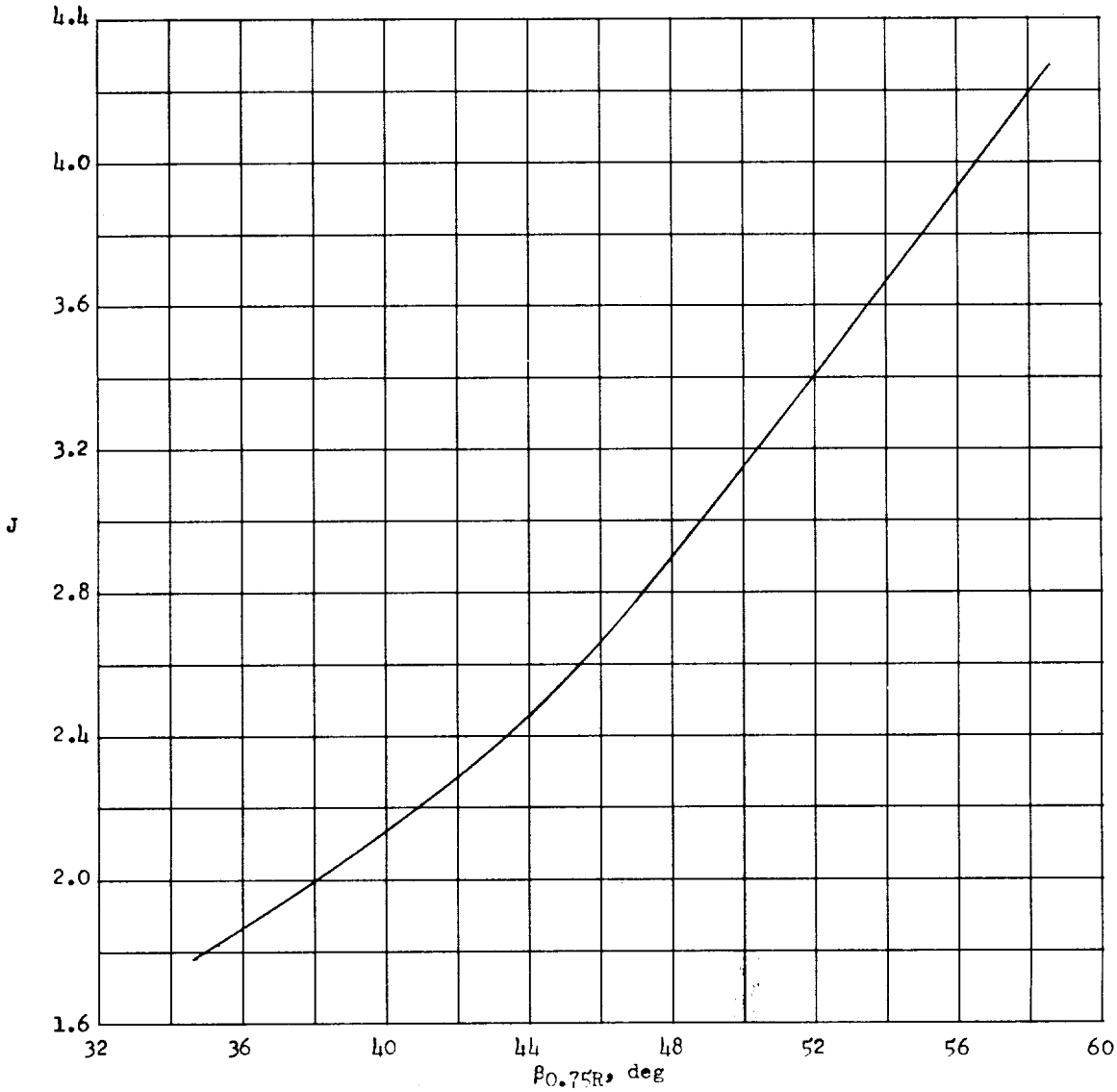


Figure 4.- Variation of advance ratio with geometric blade angle at three-quarter blade radius for windmilling propeller.

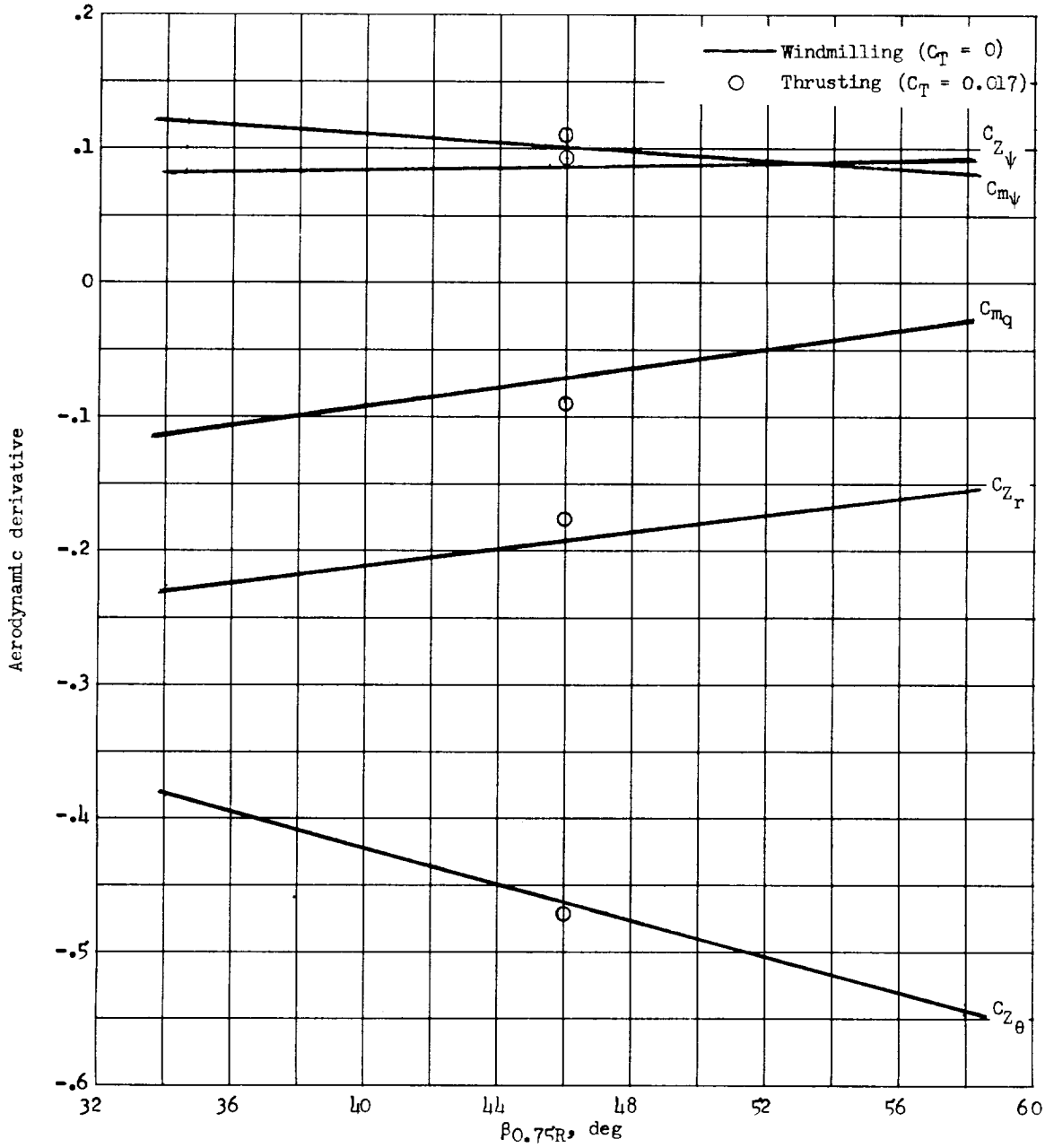


Figure 5.- Variation of propeller aerodynamic derivatives with geometric blade angle at three-quarter blade radius. M = 0.

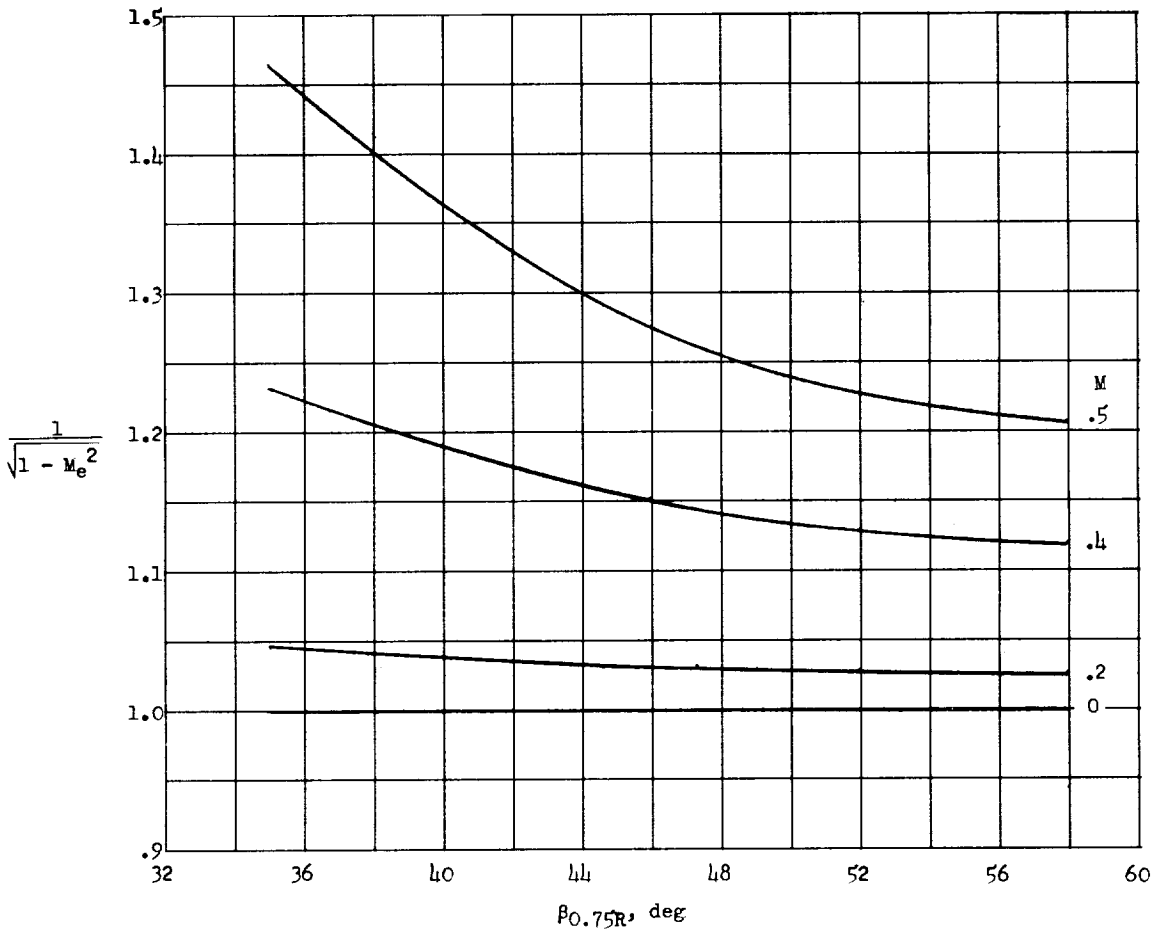


Figure 6.- Variation of Mach number correction factor for propeller aerodynamic derivatives with geometric blade angle at three-quarter blade radius.

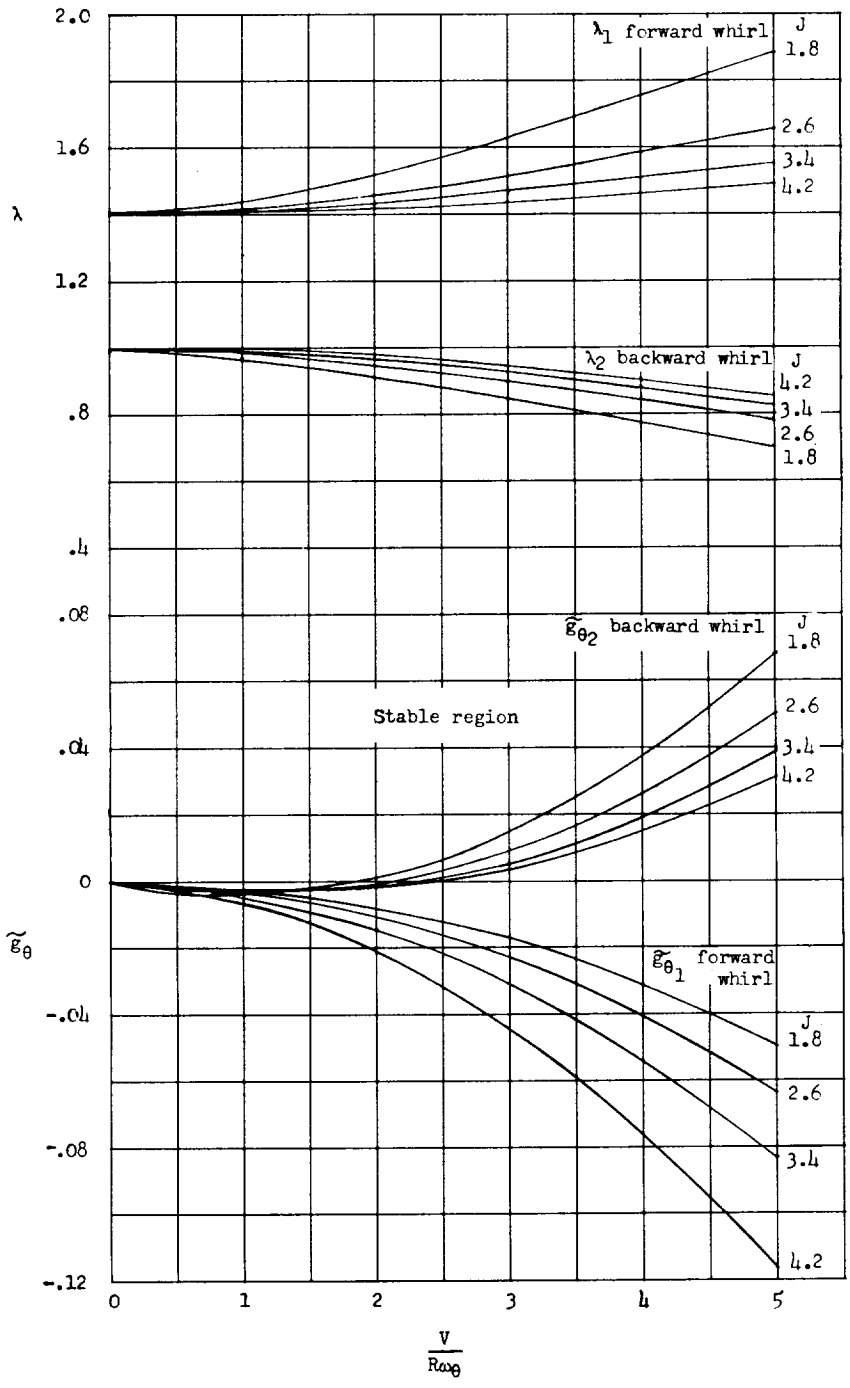


Figure 7.- Typical plots of frequency and damping required for neutral stability for various propeller advance ratios. $S_\psi/S_\theta = 1.96$; $G = 1.0$; $\gamma = 1.4$.

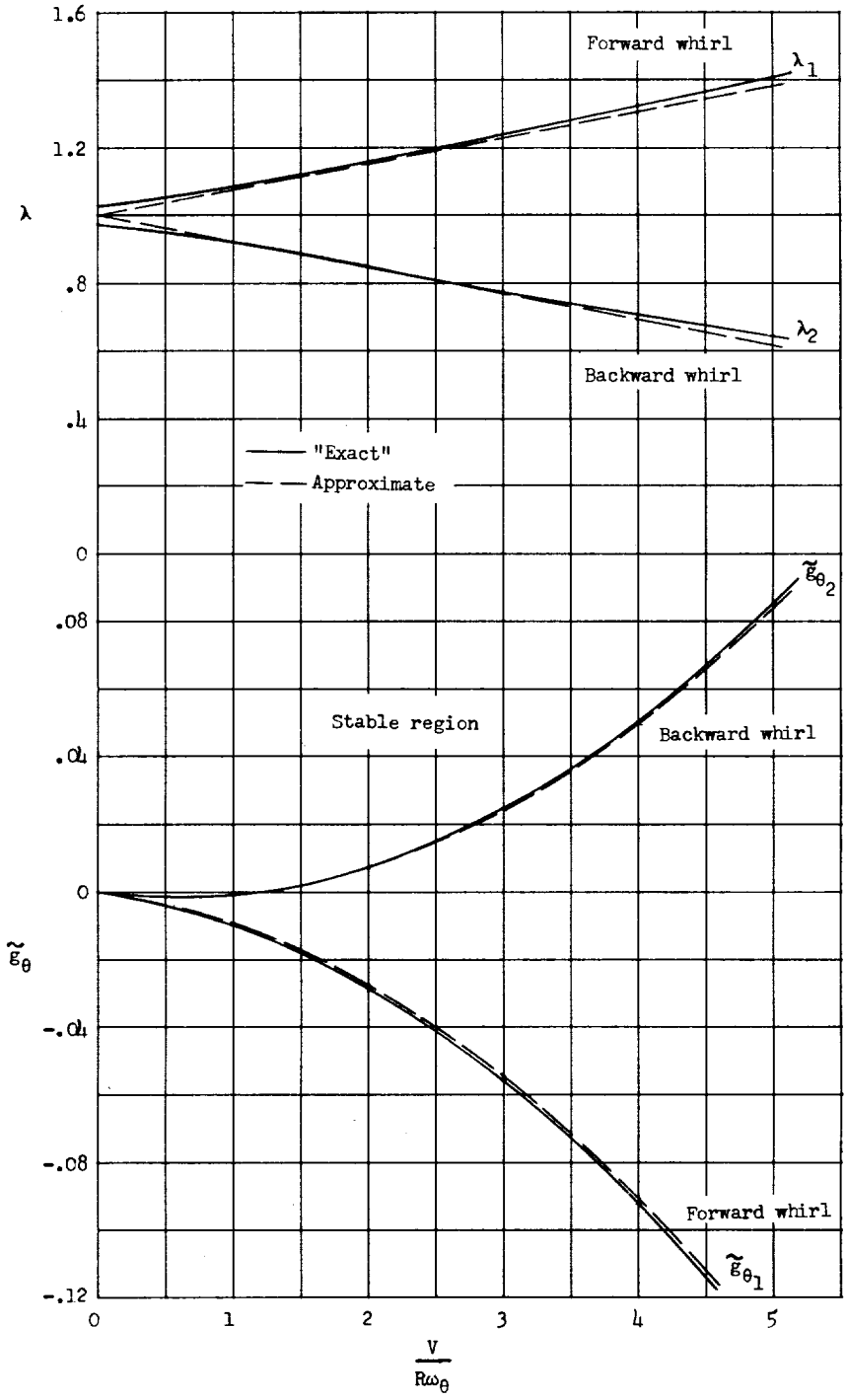


Figure 8.- Comparison of "exact" and approximate expressions for whirl frequencies and stability boundaries. J = 2.6; G = 1.0; $\gamma$ = 1.0.

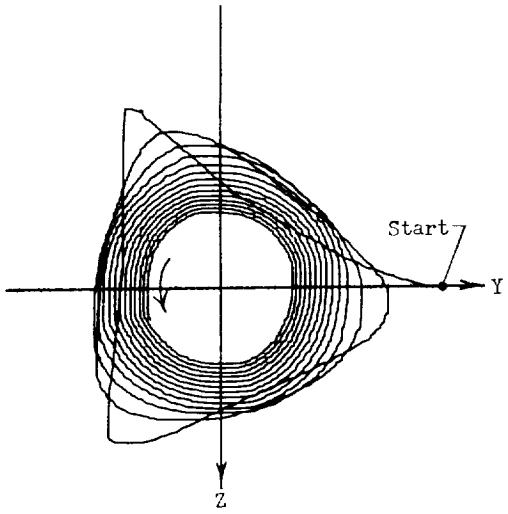


(a) Stable; $g_\theta = 0.08$.

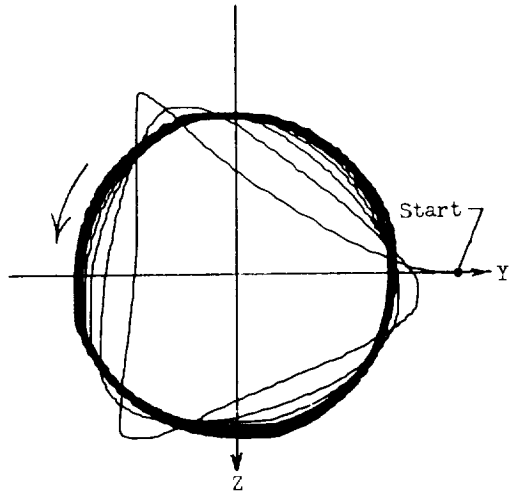


(b) Neutrally stable; $g_\theta = 0.06$.

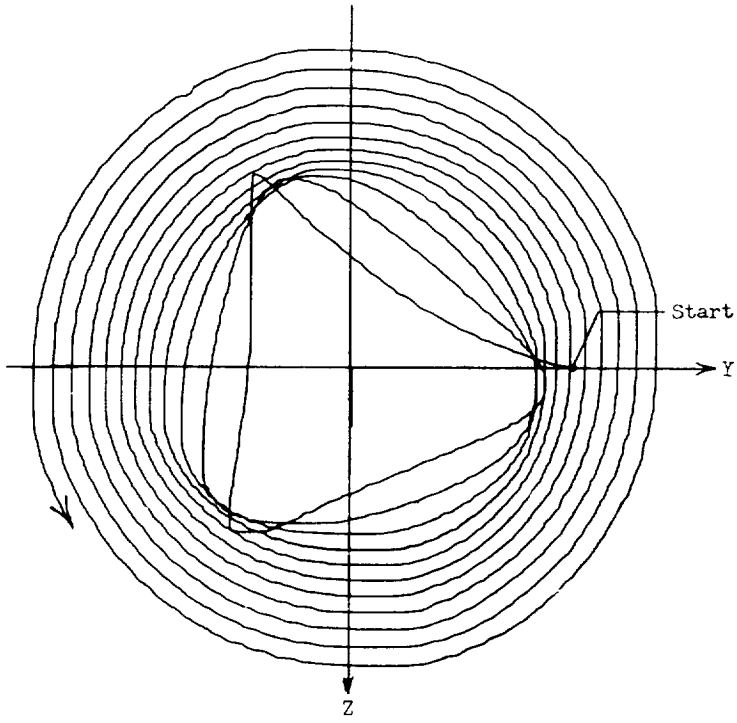


(c) Unstable; $g_\theta = 0.04$.

Figure 9.- Analog computer results showing typical paths of propeller hub following an initial lateral displacement for $G = 1.0$ and $\gamma = 1.0$. Arrows indicate direction of precession.

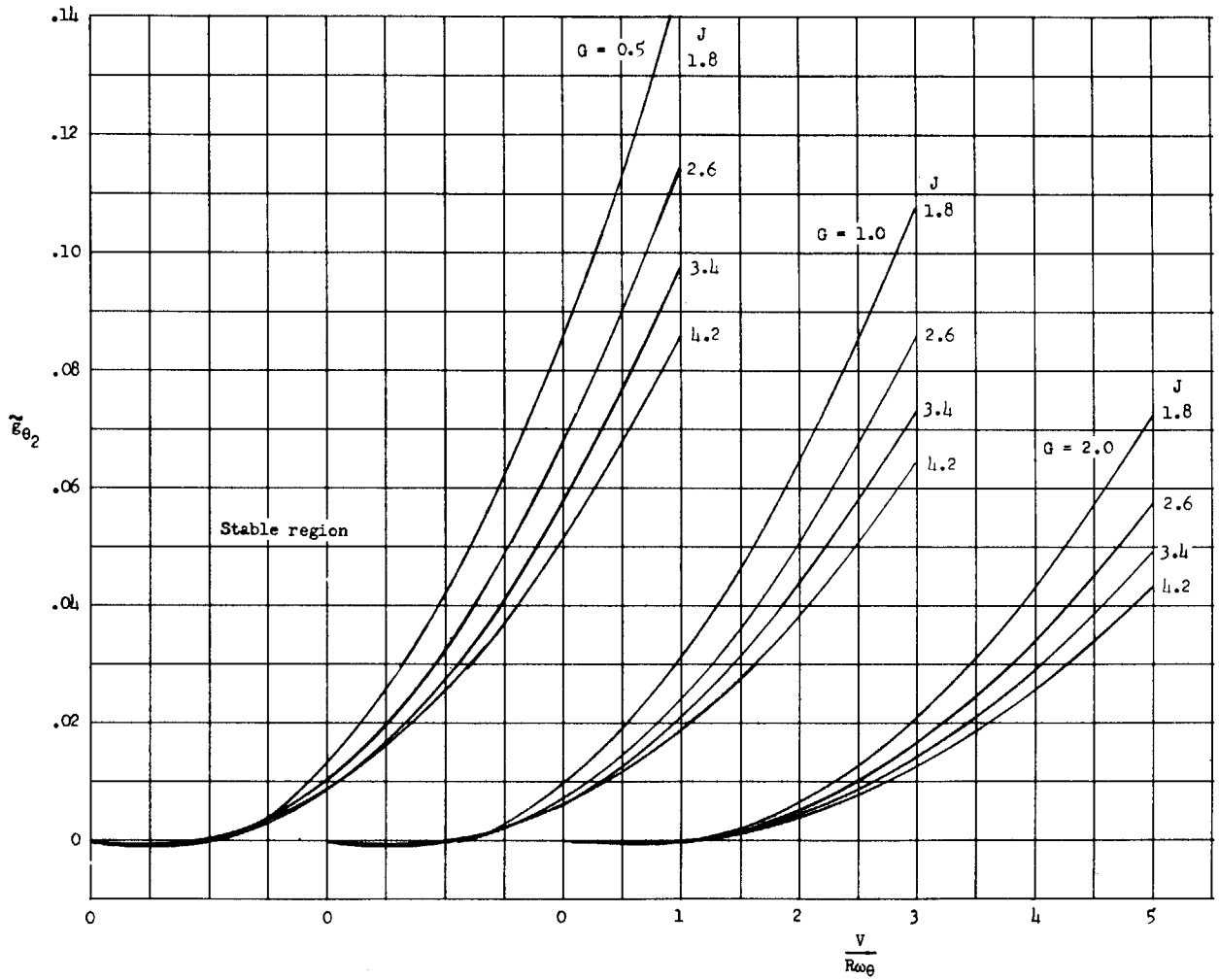


(a) $S_\psi/S_\theta = 1.0$.

Figure 10.- Nondimensional stability boundaries for the backward whirl mode.

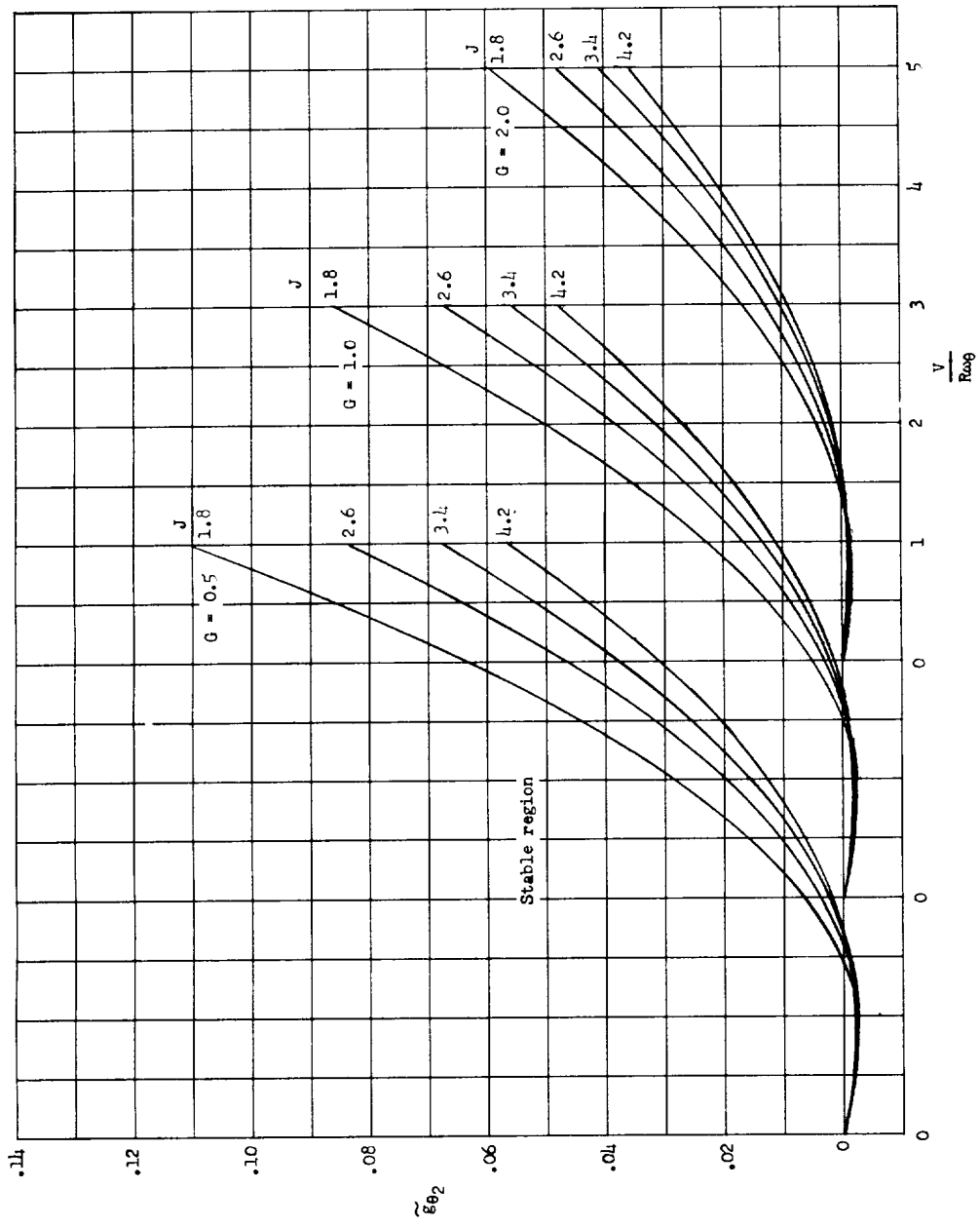


(b) $S_\psi/S_\theta = 1.44$.

Figure 10.- Continued.

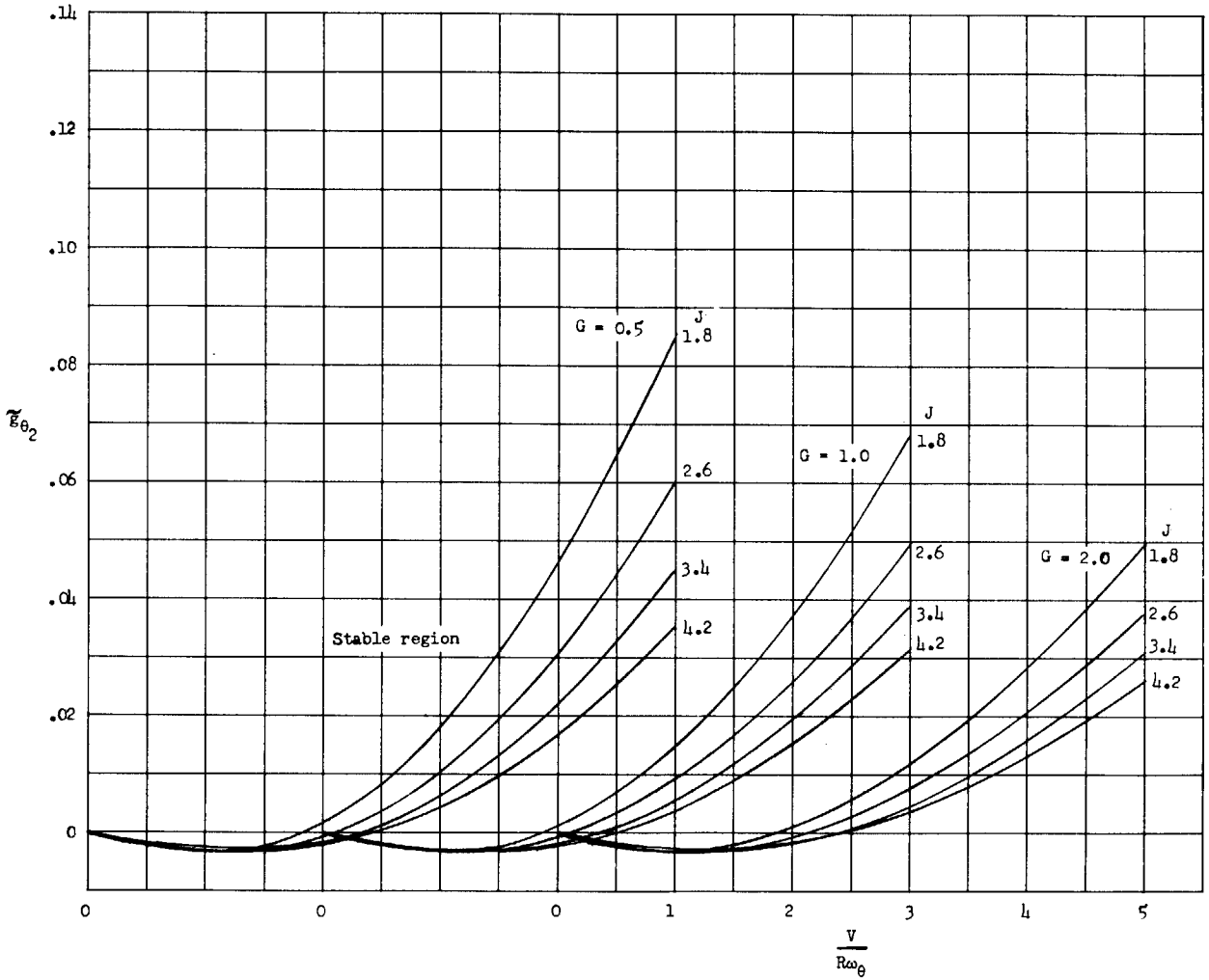


(c) $S_\psi/S_\theta = 1.96$.

Figure 10.- Continued.

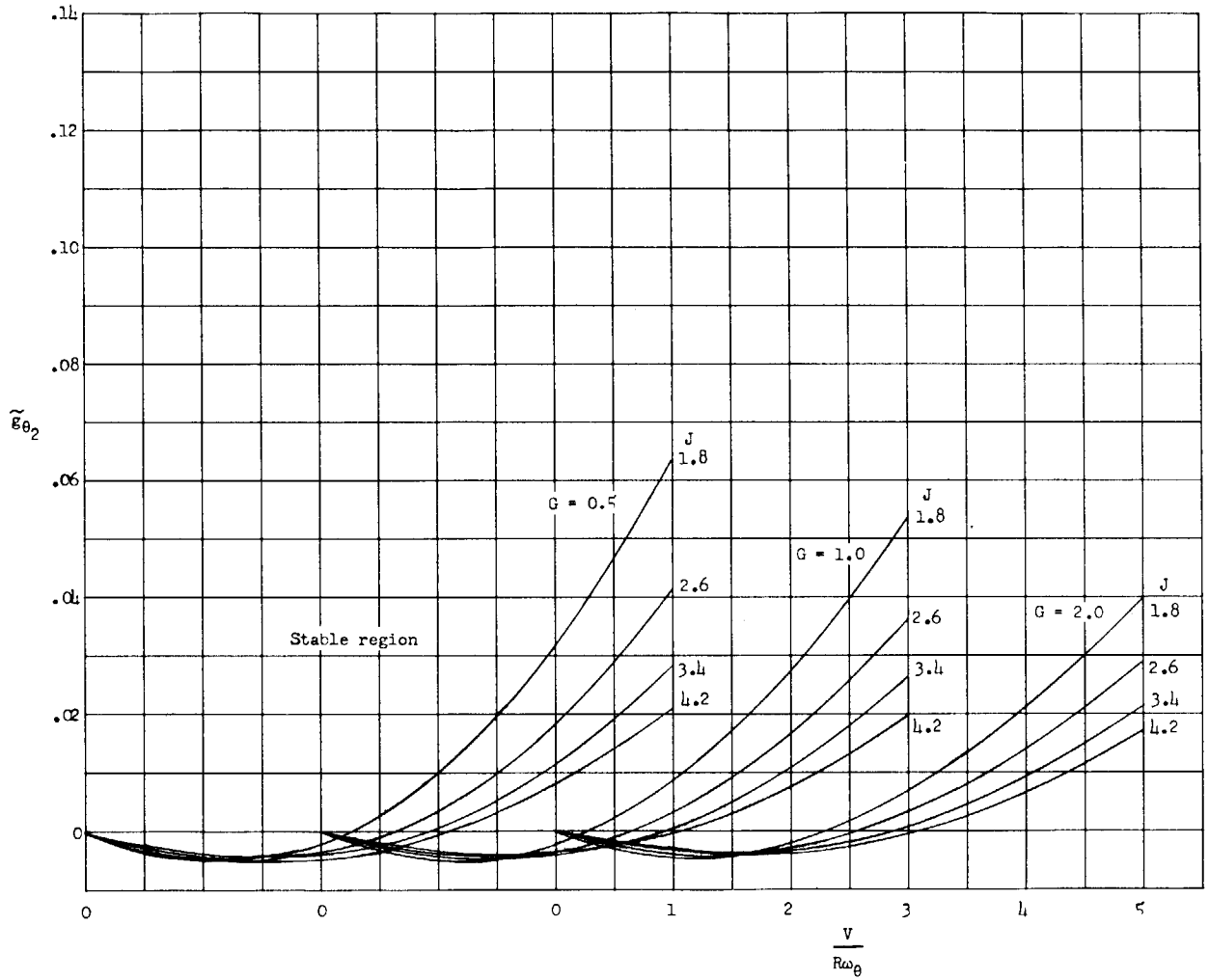


(d) $S_\psi/S_\theta = 2.56$.

Figure 10.- Concluded.

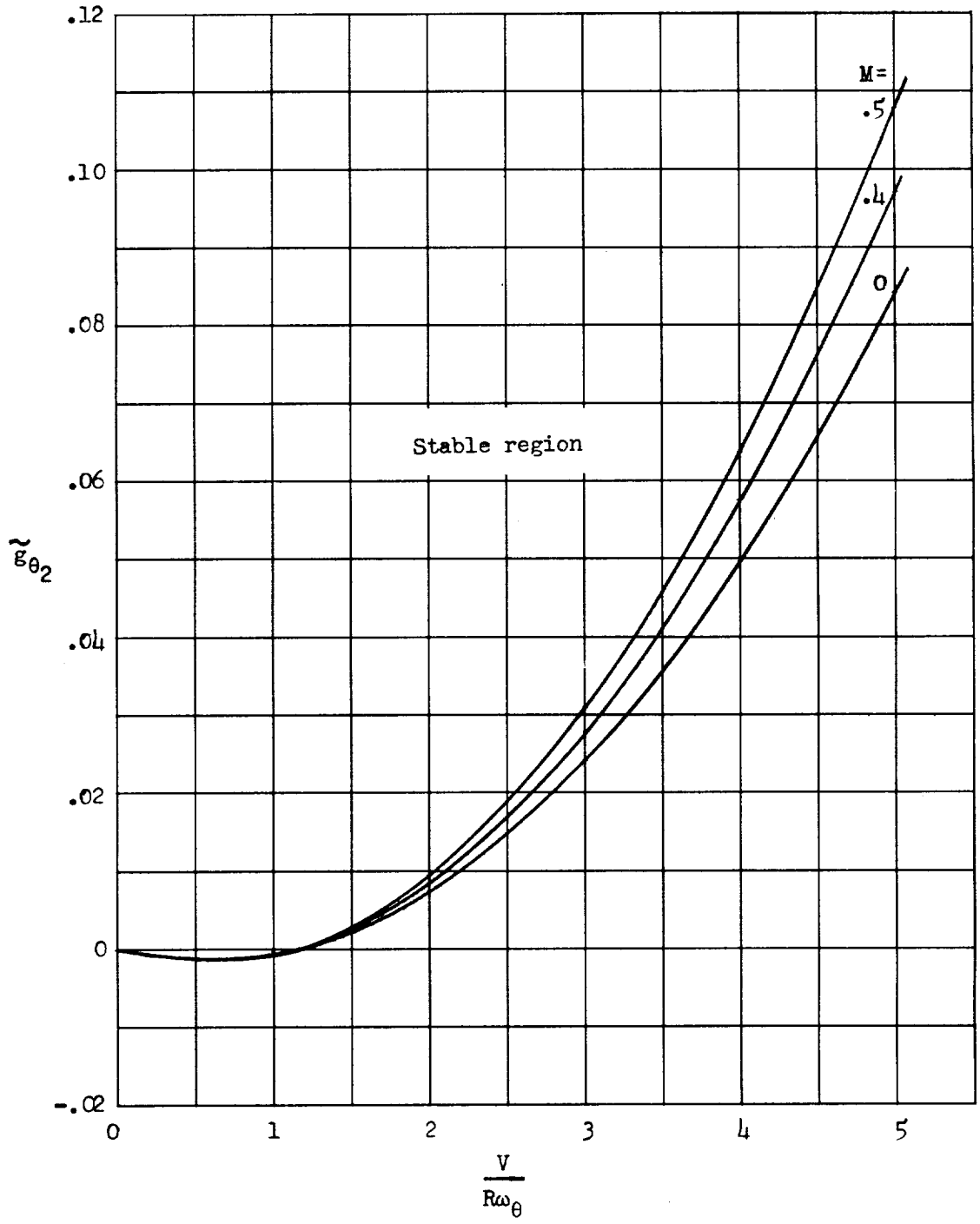


Figure 11.- Effect of Mach number on the stability boundary. J = 2.6; G = 1.0; $\gamma$ = 1.0.

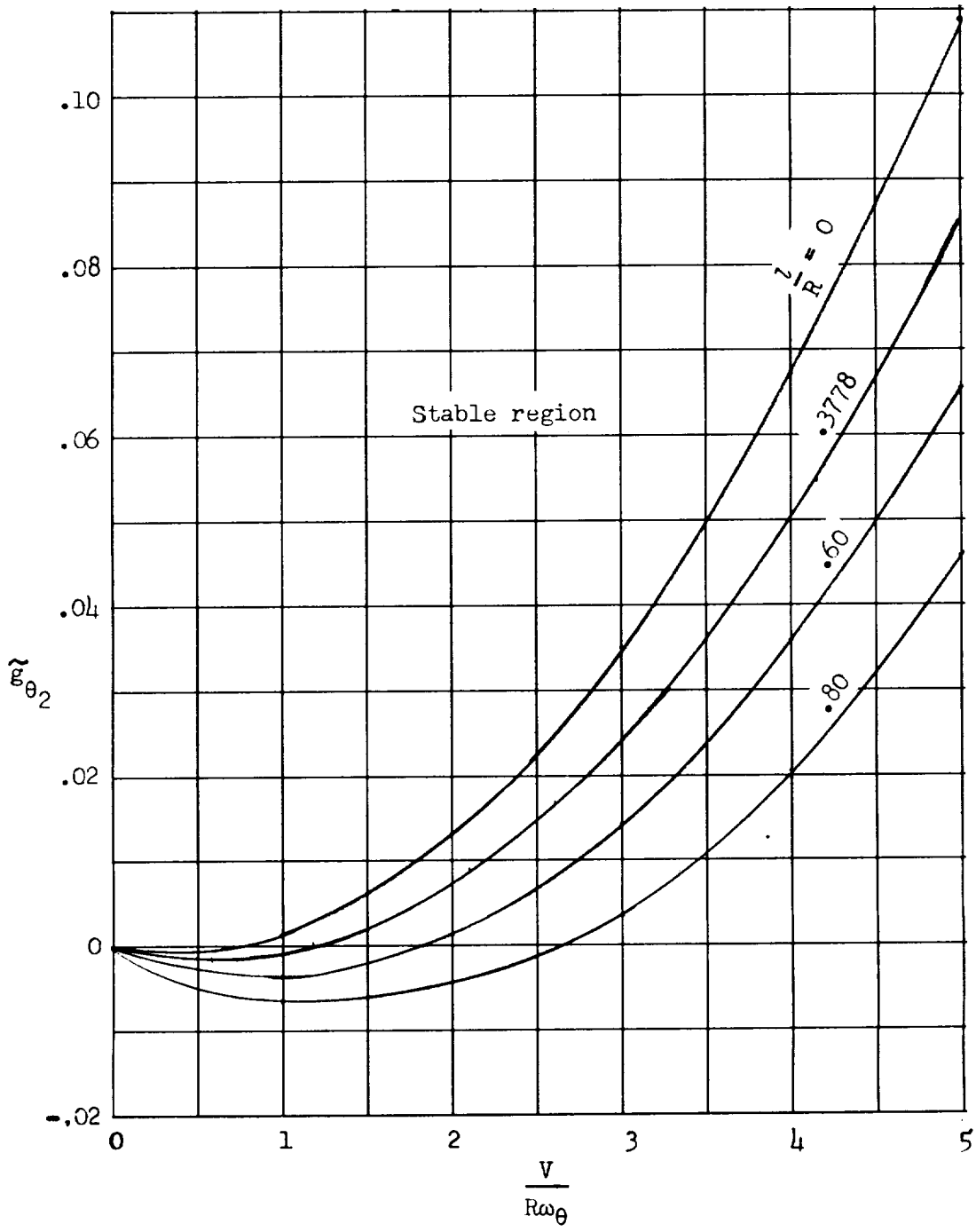


L-1297

Figure 13.- Effect of pitch-axis location on stability boundary. J = 2.6; G = 1.0; $\gamma$ = 1.0.

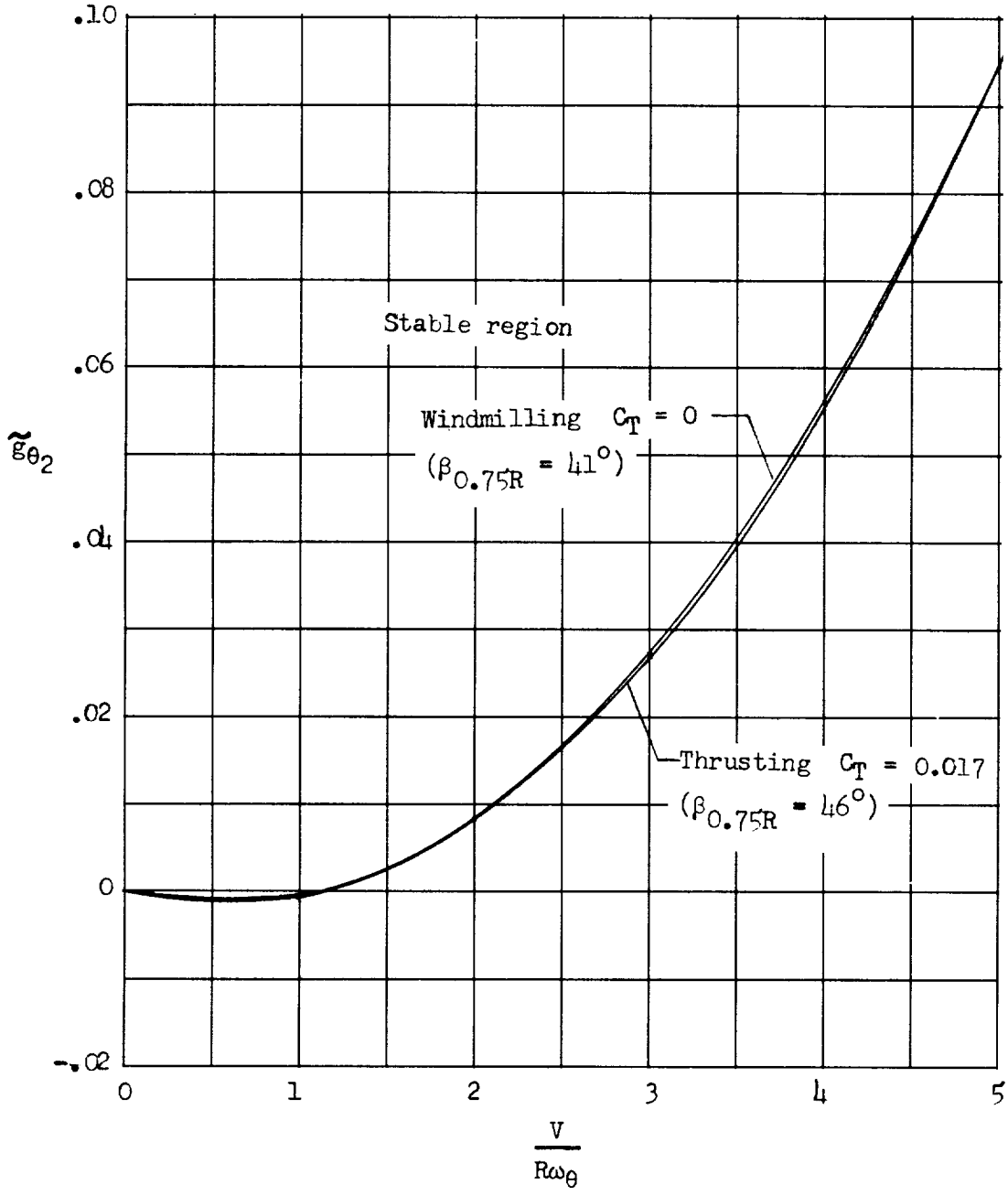


Figure 12.- A comparison of the stability boundaries for thrusting and windmilling propellers. $J = 2.22$; $G = 1.0$; $\gamma = 1.0$.

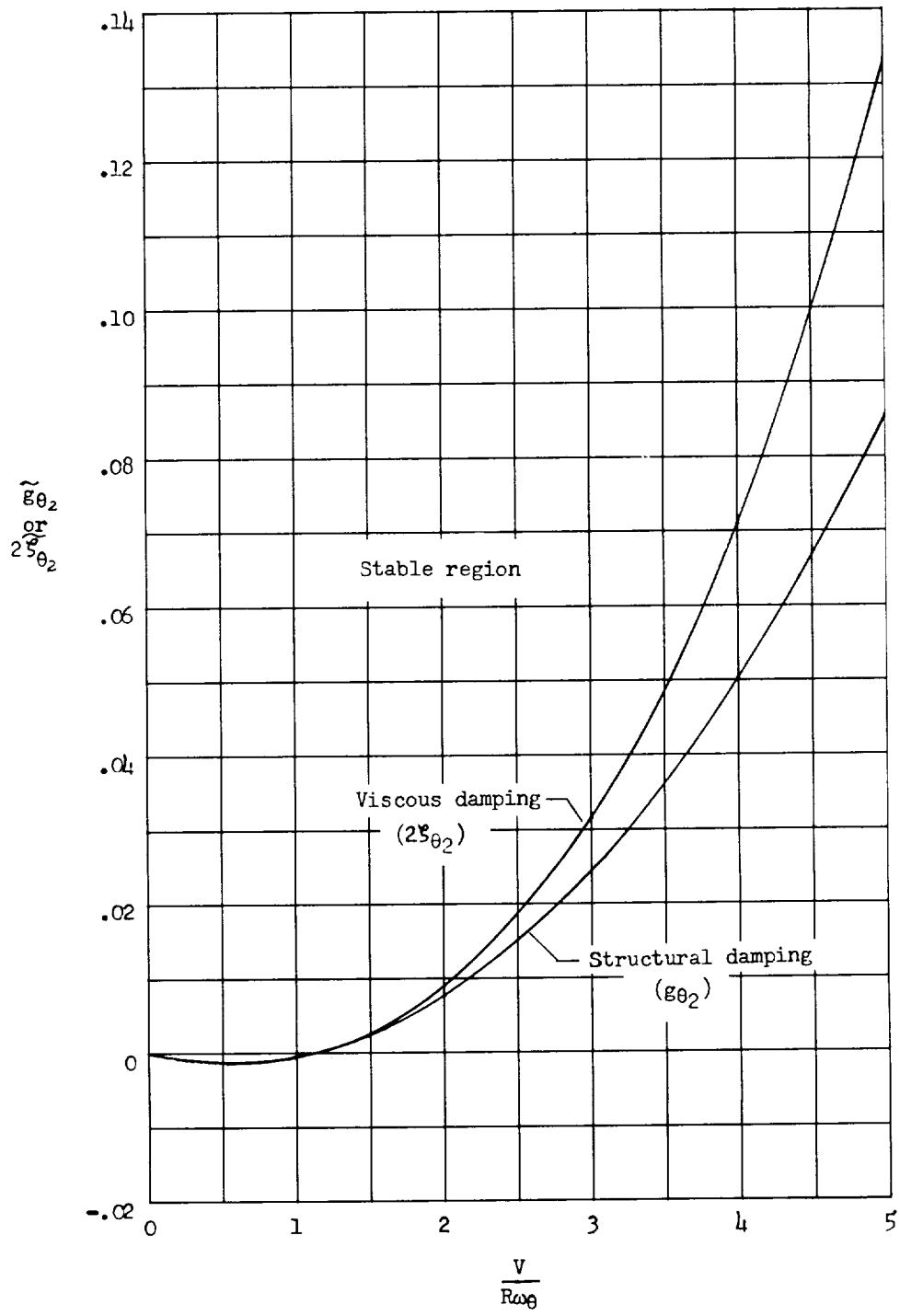


Figure 14.- Comparison of stability boundaries for viscous and structural damping. J = 2.6; G = 1.0; $\gamma$ = 1.0.

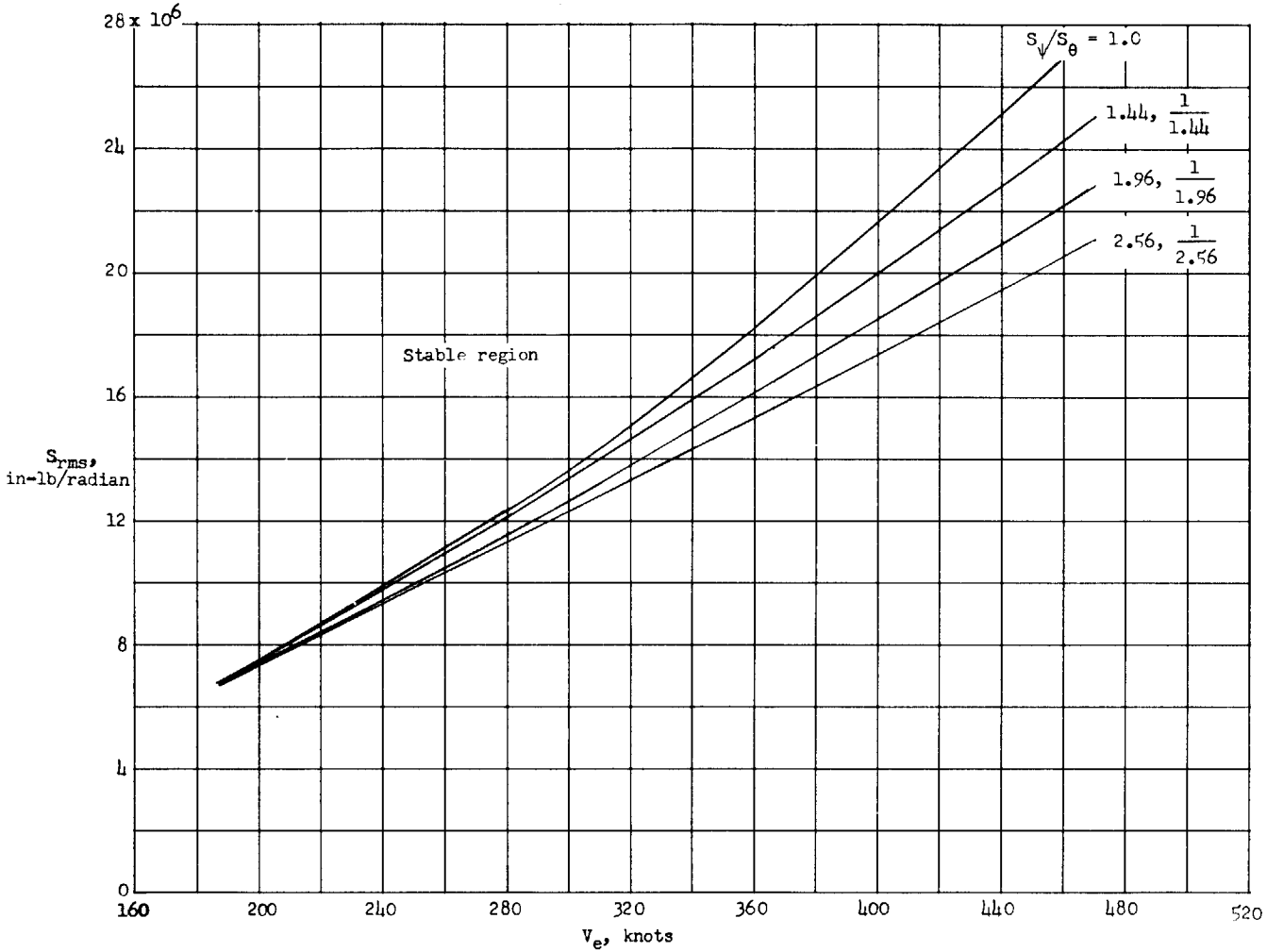


(a) Effect of stiffness ratio for unit damping ratio.

Figure 15.- Effect of stiffness and damping ratios on airspeed for propeller whirl. $\tilde{g}_{av} = 0.03$.

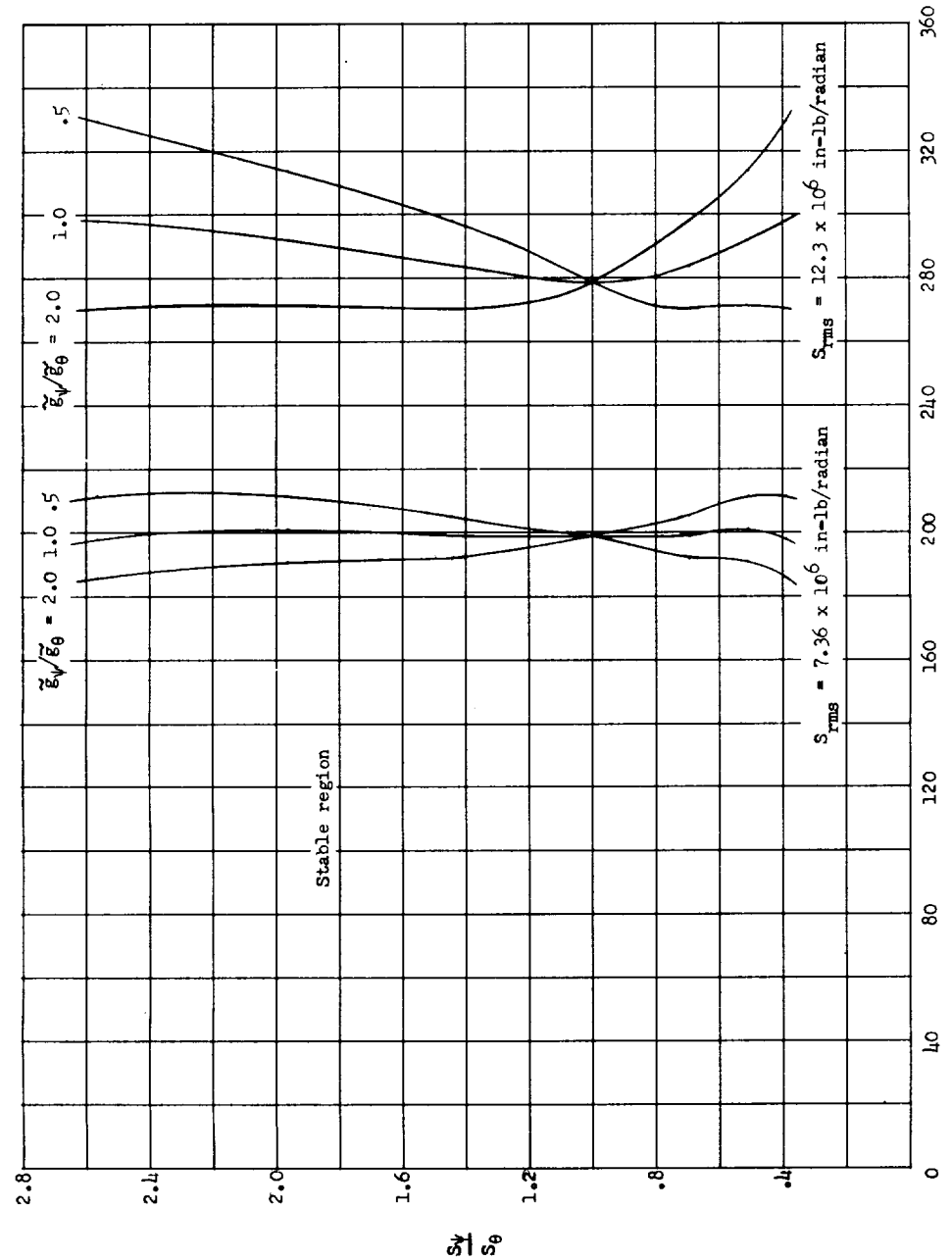


(b) Effect of damping ratio.

Figure 15.- Concluded.

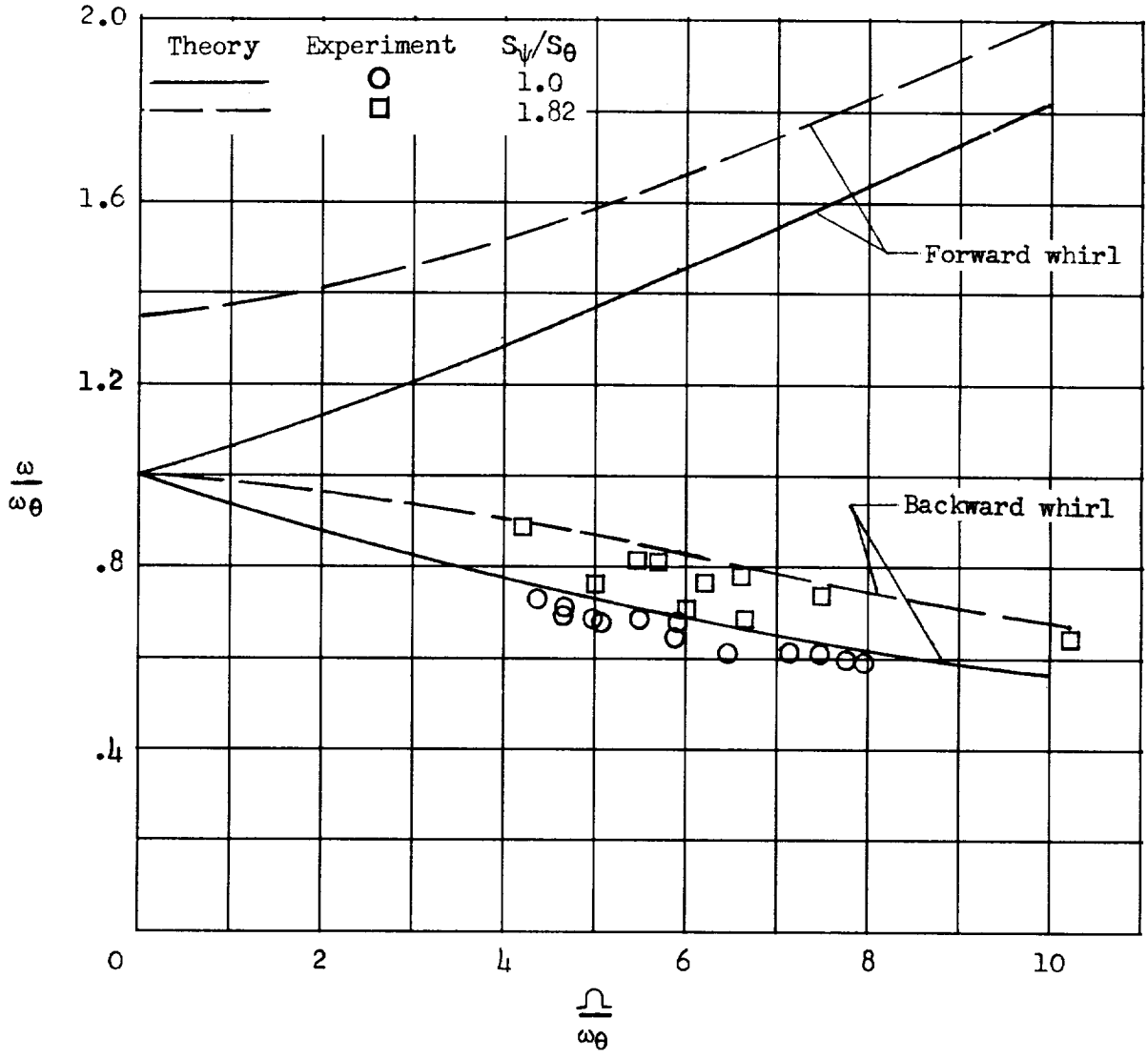


Figure 16.- Effect of propeller speed on whirl frequency for two stiffness ratios. Aerodynamic forces have been neglected in theoretical curves.

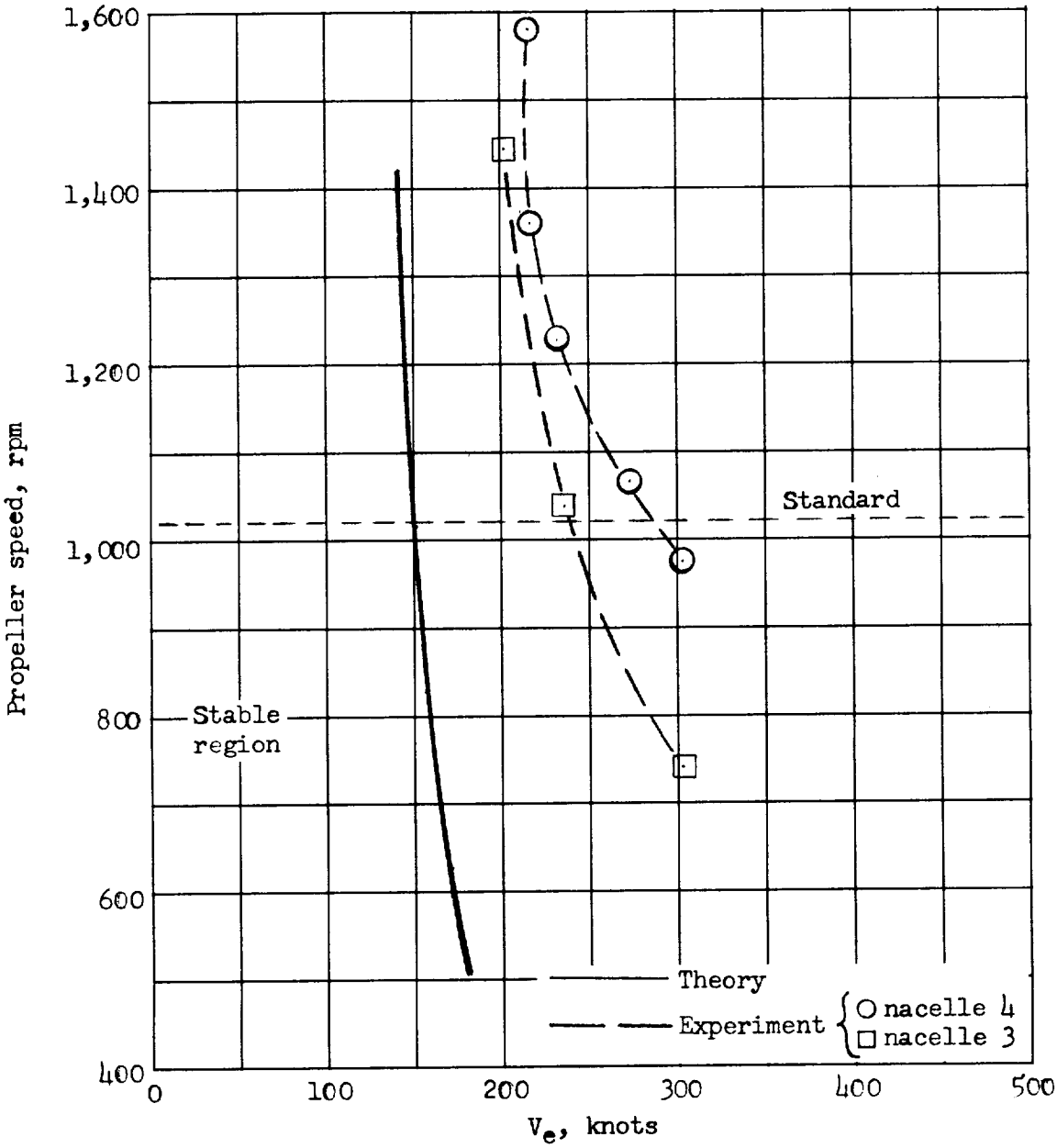


Figure 17.- Stability boundary plots of propeller speed plotted against airspeed for propeller whirl. $G = 1.0$; $\gamma = 1.0$; $g_\theta \approx 0.014$; $S_\theta = 8.09 \times 10^6$ in-lb/radian.

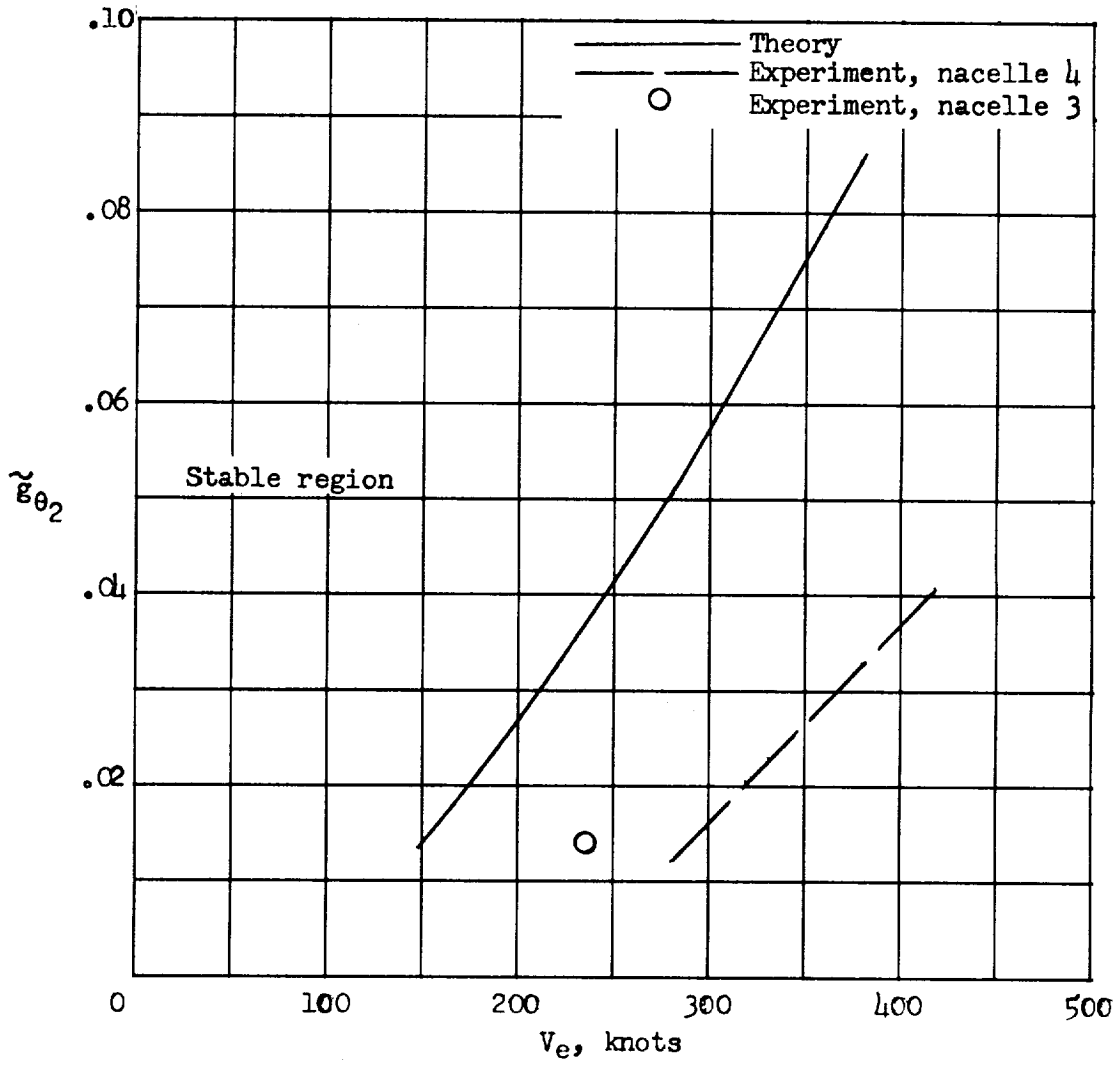


Figure 18.- Stability boundary plot of structural damping against airspeed for propeller whirl. G = 1.0; $\gamma$ = 1.0; $S_\theta$ = 8.09 × $10^6$ in-lb/radian; n = 1,020 rpm.

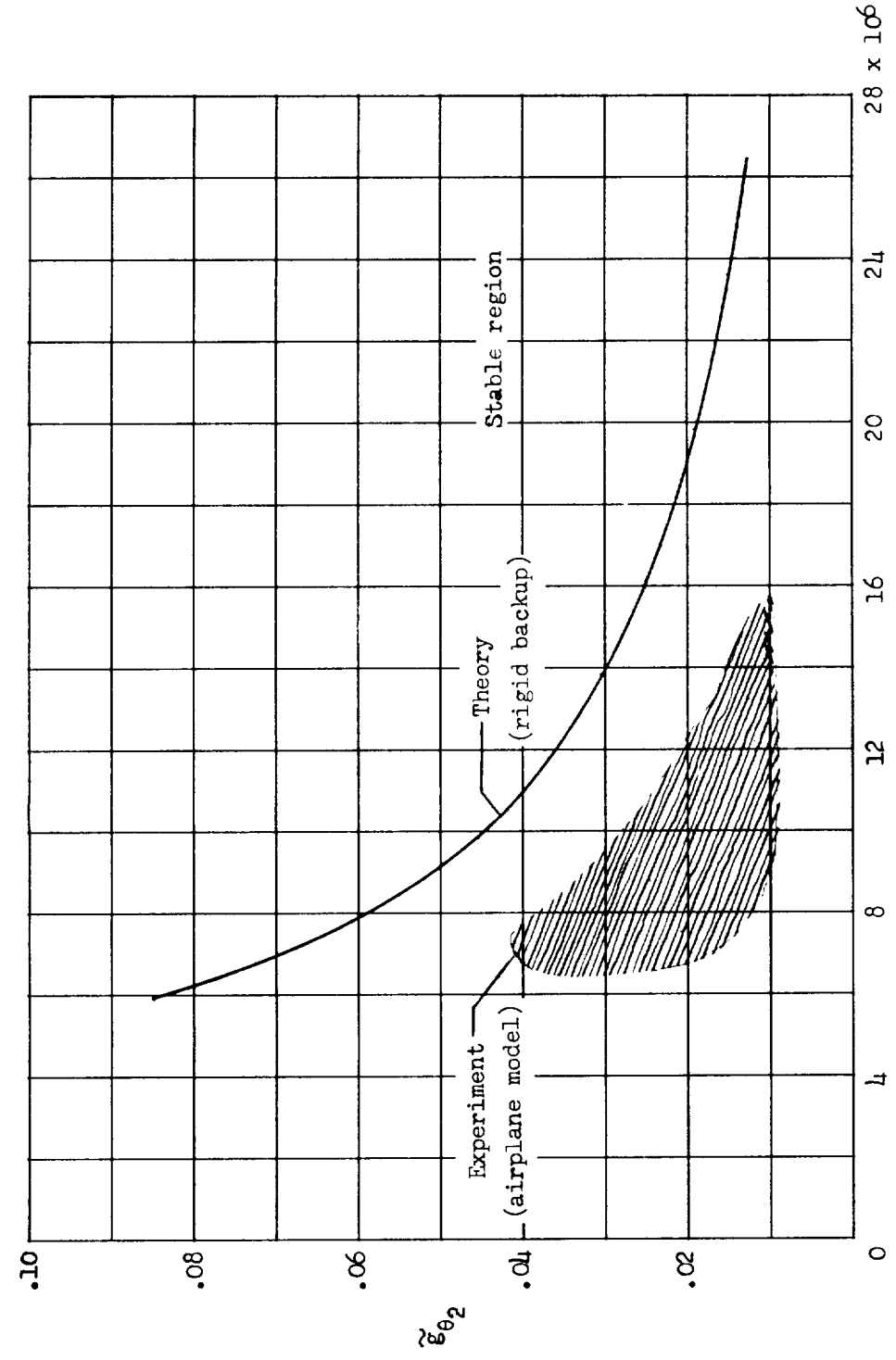


Figure 19.- Stability boundary plots of damping against root-mean-square stiffness at $V_e$ = 304 knots. G = 1.0; $\gamma$ = 1.0; n = 1,020 rpm for theoretical curve; these values vary in band of experimental data shown.

NASA TN D-659
National Aeronautics and Space Administration.
AN ANALYTICAL TREATMENT OF AIRCRAFT PROPELLER PRECESSION INSTABILITY. Wilmer H. Reed III and Samuel R. Bland. January 1961. 53p. OTS price, $1.50.
(NASA TECHNICAL NOTE D-659)

An analytical investigation has been made of the dynamic stability of an aircraft-engine—propeller combination flexibly mounted to a rigid backup structure. The conditions for which the system undergoes self-excited precession (propeller whirl) are examined. Results are presented in the form of nondimensional plots from which stability boundaries for various combinations of stiffness of the power-plant mount, structural damping, and propeller speed can be readily determined. It is found that the theoretical results, which do not account for the effects of wing response, show the same trends as observed in wind-tunnel tests of an aeroelastic model but indicate instability for lower velocities than do the model tests.
Copies obtainable from NASA, Washington

I. Reed, Wilmer H., III
II. Bland, Samuel R.
III. NASA TN D-659

(Initial NASA distribution: 51, Stresses and loads.)

NASA

NASA TN D-659
National Aeronautics and Space Administration.
AN ANALYTICAL TREATMENT OF AIRCRAFT PROPELLER PRECESSION INSTABILITY. Wilmer H. Reed III and Samuel R. Bland. January 1961. 53p. OTS price, $1.50.
(NASA TECHNICAL NOTE D-659)

An analytical investigation has been made of the dynamic stability of an aircraft-engine—propeller combination flexibly mounted to a rigid backup structure. The conditions for which the system undergoes self-excited precession (propeller whirl) are examined. Results are presented in the form of nondimensional plots from which stability boundaries for various combinations of stiffness of the power-plant mount, structural damping, and propeller speed can be readily determined. It is found that the theoretical results, which do not account for the effects of wing response, show the same trends as observed in wind-tunnel tests of an aeroelastic model but indicate instability for lower velocities than do the model tests.
Copies obtainable from NASA, Washington

I. Reed, Wilmer H., III
II. Bland, Samuel R.
III. NASA TN D-659

(Initial NASA distribution: 51, Stresses and loads.)

NASA

NASA TN D-659
National Aeronautics and Space Administration.
AN ANALYTICAL TREATMENT OF AIRCRAFT PROPELLER PRECESSION INSTABILITY. Wilmer H. Reed III and Samuel R. Bland. January 1961. 53p. OTS price, $1.50.
(NASA TECHNICAL NOTE D-659)

An analytical investigation has been made of the dynamic stability of an aircraft-engine—propeller combination flexibly mounted to a rigid backup structure. The conditions for which the system undergoes self-excited precession (propeller whirl) are examined. Results are presented in the form of nondimensional plots from which stability boundaries for various combinations of stiffness of the power-plant mount, structural damping, and propeller speed can be readily determined. It is found that the theoretical results, which do not account for the effects of wing response, show the same trends as observed in wind-tunnel tests of an aeroelastic model but indicate instability for lower velocities than do the model tests.
Copies obtainable from NASA, Washington

I. Reed, Wilmer H., III
II. Bland, Samuel R.
III. NASA TN D-659

(Initial NASA distribution: 51, Stresses and loads.)

NASA

NASA TN D-659
National Aeronautics and Space Administration.
AN ANALYTICAL TREATMENT OF AIRCRAFT PROPELLER PRECESSION INSTABILITY. Wilmer H. Reed III and Samuel R. Bland. January 1961. 53p. OTS price, $1.50.
(NASA TECHNICAL NOTE D-659)

An analytical investigation has been made of the dynamic stability of an aircraft-engine—propeller combination flexibly mounted to a rigid backup structure. The conditions for which the system undergoes self-excited precession (propeller whirl) are examined. Results are presented in the form of nondimensional plots from which stability boundaries for various combinations of stiffness of the power-plant mount, structural damping, and propeller speed can be readily determined. It is found that the theoretical results, which do not account for the effects of wing response, show the same trends as observed in wind-tunnel tests of an aeroelastic model but indicate instability for lower velocities than do the model tests.
Copies obtainable from NASA, Washington

I. Reed, Wilmer H., III
II. Bland, Samuel R.
III. NASA TN D-659

(Initial NASA distribution: 51, Stresses and loads.)

NASA